

How alkaline compounds control atmospheric aerosol acidity

Vlassis A. Karydis^{1,2*}, Alexandra P. Tsimpidi^{1,2,3}, Andrea Pozzer^{1,4}, and Jos Lelieveld^{1,5}

¹ Max Planck Institute for Chemistry, Atmospheric Chemistry Dept., Mainz, 55128, Germany.

² Forschungszentrum Jülich, Inst. for Energy and Climate Research, IEK-8, Jülich, 52425, Germany.

³ National Observatory of Athens, Inst. for Environmental Research and Sustainable Development, Athens, 15236, Greece.

⁴ International Centre for Theoretical Physics, Trieste, 34151, Italy

⁵ The Cyprus Institute, Climate and Atmosphere Research Center Nicosia, 1645, Cyprus.

Correspondence to: Vlassis A. Karydis (v.karydis@fz-juelich.de)

Abstract. The acidity of atmospheric aerosols regulates the particulate mass, composition and toxicity, and has important consequences for public health, ecosystems and climate. Despite these broad impacts, the global distribution and evolution of aerosol acidity are unknown. We used the ~~particular~~, comprehensive atmospheric multiphase chemistry – climate model EMAC to investigate the main factors that control aerosol acidity; and uncovered remarkable variability and unexpected trends during the past 50 years in different parts of the world. We find that alkaline compounds, notably ammonium, and to a lesser extent crustal cations, ~~buffer~~regulate the aerosol pH on a global scale. Given the importance of aerosols for the atmospheric energy budget, cloud formation, pollutant deposition and public health, alkaline species hold the key to control strategies for air quality and climate change.

1. Introduction

Aerosol acidity is a central property of atmospheric particulates that influence clouds, climate and air quality, including impacts on human health (Raizenne et al., 1996; Lelieveld et al., 2015). It affects the partitioning of semi-volatile acids between the gas and aerosol phases (Guo et al., 2016; Guo et al., 2017; Guo et al., 2018; Nenes et al., 2020), secondary organic aerosol (SOA) formation (Xu et al., 2015; Marais et al., 2016), the solubility of trace metals in aerosols (~~Oakes et al., 2012~~)(Oakes et al., 2012), associated with their toxicity (~~Fang et al., 2017~~)(Fang et al., 2017) and nutrient capacity (Jickells et al., 2005), the activation of halogens that act as oxidants (Saiz-Lopez and von Glasow, 2012), the conversion of sulfur dioxide (Seinfeld and Pandis, 2006; Cheng et al., 2016), the particle hygroscopic growth and lifetime (Metzger et al., 2006; Abdelkader et al., 2015; Karydis et al., ~~2016~~2017), and atmospheric corrosivity (Leygraf et al., 2016). Direct measurement of aerosol acidity is difficult and associated with much uncertainty, being dependent on filter sampling and the H⁺ molality in the aqueous extract, which is sensitive to artifacts (~~Pathak et al., 2004~~)(Pathak et al., 2004). Therefore, particle

30 pH, a commonly used acidity metric of aqueous aerosols, is typically inferred by proxy techniques (Hennigan et al.,
31 2015;Pye et al., 2020). Two of the most common are the ion balance and the molar ratio methods. ~~In the past, these~~These
32 methods ~~did~~do not consider the effects of aerosol water and multiphase interactions with gas phase species as well as the
33 partial dissociation of acids (Hennigan et al., 2015). The simultaneous measurement of gas phase species can improve
34 aerosol pH estimates by accounting for the phase partitioning of semi-volatile species (e.g., NH₃, HNO₃). However, the
35 accuracy of this approach relies on the availability of information on these species in both the gas and aerosol phase, being
36 scant in most cases.

37 The bestmost reliable estimates of pH are obtained with thermodynamic equilibrium models, although the accuracy can be
38 limited by not accounting for all ionic species. For example, most atmospheric chemistry models do not consider crustal
39 elements (e.g., Ca²⁺, Mg²⁺, K^{+/-}) and Na⁺ in sea salt. These species affect the ion balance by influencing the phase
40 partitioning of nitrate and ammonium, especially in areas where aeolian dust is abundant (Karydis et al., 2016). Here we
41 present 50-year global acidity trends of fine aerosols (i.e. with a diameter < 2.5 μm) by employing the EMAC chemistry –
42 climate model (Jöckel et al., 2010). The pH calculations are performed online with the ISORROPIA II thermodynamic
43 equilibrium model (Fountoukis and Nenes, 2007).

44 2. Results and Discussion

45 2.1 Global variability of aerosol acidity

46 Figure 1 shows the modeled near-surface distribution of fine aerosol acidity for the 2010-2015 period. We find
47 predominantly acidic particles over the anthropogenically influenced regions in the northern hemisphere and the tropical
48 biomass burning zones, and mostly alkaline particles over deserts and oceans, especially over the southern oceans. The pH
49 typically ranges from 4.0 to 6.7 (5.3 on average) over the western USA since it is affected by crustal cations from the
50 surrounding deserts. ~~Therefore,~~Polluted areas located downwind of crustal sources are of special interest since the pH
51 calculations ~~in this region are can be~~ sensitive to the aerosol state assumption. ~~(see section 4.3)~~. Over Pasadena, the base case
52 model using the stable state mode estimates a mean pH of 5.9 units, while the sensitivity simulation with only liquid aerosols
53 results in 2.7 pH units (equal to Guo et al. (2017) estimations by using the metastable assumption; Table S1). Our sensitivity
54 analysis revealed that the aerosol state itself is not affected by the state assumption since both stable and metastable predict
55 the same amount of water in the aerosol. Differences in the calculated pH can be due to the high concentrations of calcium
56 from the Great Basin Desert which results in the precipitation of high amounts of CaSO₄, lowering the particle acidity (but
57 without affecting the water activity since CaSO₄ is insoluble and does not contribute to the MDRH depression). It is worth
58 mentioning that calcium was not included in the Guo et al. (2017) study which helps explain the differences in the observed
59 and simulated aerosol acidity. The simulated particle-phase fraction of nitrate over Pasadena is 40% using the stable state
60 assumption and 32% using the metastable assumption, compared to the observationally derived 51%. Over Europe, the pH

61 ranges from 2.6 to 6.7 (3.9 on average). Observational estimates of aerosol pH from the Po Valley (Squizzato et al.,
62 2013; Masiol et al., 2020) and Cabauw (Guo et al., 2018) support the relatively low acidity of fine aerosols over Europe
63 (Table S1). Model calculations compare well with observational estimates from Cabauw, however, result in higher pH (~1
64 unit) compared to values from Po Valley (estimated by using the E-AIM model). Over East Asia the average pH is 4.7,
65 ranging from 2.6 to 7.4. Relatively high pH^{spH} are found over regions where anthropogenic aerosols are mixed with
66 aeolian dust, e.g., from the Gobi Desert, which ~~bufferdecrease~~ the acidity (e.g., ~6 pH units over Hohhot, which agrees well
67 with the estimations of Wang et al. (2019a)). The relatively low pH in large parts of Asia is explained by strong SO_2
68 emissions and associated sulfate, which have increased strongly in the past decades (e.g., over Guangzhou, supported by
69 estimations of Jia et al. (2018)). Estimates of unrealistically high aerosol acidity can result from omitting the gas phase
70 concentrations of semi-volatile ions from the pH calculations (e.g., estimates over Hong Kong (Yao et al., 2007; Xue et al.,
71 2011), Singapore (Behera et al., 2013) and Shanghai (Pathak et al., 2009); Table S1). At the same time, SO_2 emissions have
72 decreased over Europe and USA, and recently in China. However, aerosols over the eastern USA have remained acidic, with
73 an average pH of 3.0 until recently, corroborating the findings of Weber et al. (2016) and Lawal et al. (2018) that aerosol
74 acidity over this region is less sensitive to SO_2 than to NH_3 emissions.

75 The aerosol pH over ~~the anthropogenically influenced/polluted~~ northern hemispheric mid-latitudes (e.g., over East Asia) and
76 ~~the northern extratropical oceans~~ exhibits a clear seasonal pattern with lower values during boreal summer and higher ones
77 during winter, driven by the availability of ammonium and by the aerosol water content (Fig. 2). This is evident from both
78 our model calculations and from observational estimates mostly in heavily populated areas such as the Po Valley (Squizzato
79 et al., 2013), Beijing (Tan et al., 2018), and Tianjin (Shi et al., 2017), and to a lesser extent over areas strongly affected by
80 aeolian dust (e.g., Hohhot; Wang et al., 2019b) (Table S1). Over tropical regions, fine particulates have a pH between 3.2
81 and 7.4, being strongly influenced by pyrogenic potassium, i.e., from widespread biomass burning (Metzger et al., 2006),
82 and a high aerosol water content. Observational estimates from Sao Paulo support these high pH values (Vieira-Filho et al.,
83 2016), albeit with 1 unit bias mainly related to the use of the E-AIM model. Over deserts, aerosols are relatively alkaline,
84 with a pH up to 7.4. Aerosols in the marine environment tend to be alkaline also, with a pH up to 7.4 over the southern
85 oceans. Observational estimates report highly acidic aerosols over the southern oceans due to the lack of gas phase input for
86 the pH calculations (Dall'Osto et al., 2019). Over the Arctic and the northern Atlantic and Pacific Oceans, aerosol acidity is
87 significantly enhanced by strong sulfur emissions from international shipping and pollution transport from industrialized
88 areas- (Fig. 1). The pH over the northern extratropical oceans and the Arctic ranges from 2.0 to 7.0 with an average of about
89 5.2. The annual cycle of aerosol acidity over these regions is strongly influenced by anthropogenic pollution, being relatively
90 high during boreal summer. Over the Antarctic, aerosol pH ranges from 4.5 to 7.0 and follows a clear seasonal pattern (Fig.
91 2).

92 2.2 Temporal evolution of aerosol acidity

93 Figure 1 and Table 1 present the aerosol pH over the period 1970-2020. We investigated the impacts of alkaline species by
94 omitting the emissions of ammonia and mineral cations in two sensitivity simulations.

95 2.2.1 Europe

96 Over Europe, the pH has increased strongly from about 2.8 during the 1970s to 3.9 recently. Especially during the 1990s
97 NH₃ emissions over Europe increased significantly by 14%, while at the same time NO_x and SO₂ emissions decreased by
98 13% and 49%, respectively. While this trend has continued in the past decade, pH changes slowed because the sulfate and
99 nitrate decreases have been compensated through volatilization of ammonia from the particles. In addition, the recently
100 increasing cation/anion ratio is accompanied by a reduction of aerosol water, preventing a significant decrease of the aerosol
101 acidity (Fig. S1). Overall, the increase of aerosol pH by more than 1 unit during the last 50 years had a significant impact on
102 the gas-particle partitioning of semi-volatile acids, e.g., nitric acid, since their dissociation into ions enhances their solubility
103 (Nah et al., 2018). Here, the fraction of nitrate in the particle phase relative to total nitrate (gas plus particle) has increased
104 from ~70% to 85% (Fig. 3). The increase in aerosol pH has been accompanied by an increase in aerosol κ
105 hygroscopicity (Fig. 4). After the substantial reduction of SO₂ emissions, sulfate salts (e.g., ammonium sulphate sulfate with
106 $\kappa=0.53$) are replaced by more hygroscopic nitrate salts (e.g., ammonium nitrate with $\kappa=0.67$) in the aerosol
107 composition. In addition, the decrease of organic compound emissions during the last 50 years contributed to the increase of
108 the aerosol hygroscopicity. Our sensitivity simulations reveal that aerosol acidity over Europe is highly sensitive to NH₃
109 emissions. Despite the decline of both SO₂ and NO_x during the past decades, the aerosol would have remained highly acidic
110 (pH ~1) in the absence of NH₃.

111 2.2.2 North America

112 Over North America, aerosol acidity also decreased with SO₂ and NO_x emissions. Nevertheless, these emissions are still
113 relatively strong in the eastern USA (5 times higher than in the western USA) resulting in very acidic aerosols, with a pH
114 ranging from 2.2 in 1971 to 3.3 recently (Figs. 1 and S1). Such acidic conditions promote the dissolution of metals (e.g., Fe,
115 Mn, Cu) in ambient particles (Fang et al., 2017)(Fang et al., 2017). Soluble transition metals in atmospheric aerosols have
116 been linked to adverse health impacts since they generate reactive oxygen species, leading to oxidative stress and increased
117 toxicity of fine particulate matter (Fang et al., 2017; Park et al., 2018). Since the solubility of transition metals increases
118 exponentially below a pH of 3, the decrease of aerosol acidity over the eastern USA reported here suggests that the particles
119 have become substantially less toxic in the past few decades. Similar to Europe, the increasing pH has resulted in a growing
120 aerosol nitrate fraction from ~50% during the 1970s to 65% recently (Fig. 3), and to a strong increase of aerosol
121 hygroscopicity by ~0.15 units at the cloud base (Fig. 4). The role of NH₃ is critically important; without it the aerosol pH

122 over the eastern USA would be close to zero. Over the western USA, the aerosol pH is higher (~5), being affected by aeolian
123 dust from the Great Basin Desert, although NH₃ is still the most important alkaline buffer.

124 2.2.3 East and South Asia

125 In Asia, SO₂ and NO_x emissions have increased drastically since 1970. However, the simultaneous increase of NH₃
126 emissions along with the presence of mineral dust from the surrounding deserts (i.e., Gobi, Taklimakan, Thar) decelerated
127 the increase of aerosol acidity. Over East Asia, the aerosol pH decreased from about 5.3 during the 1970s to 4.5 in 2010.
128 This change in aerosol acidity has affected the predominant pathway of sulfate formation through ~~aqueous-phase chemistry.~~
129 ~~Under acidic conditions, SO₂ is mainly oxidized by dissolved H₂O₂, while at pH > 5 the oxidation by O₃ predominates~~
130 ~~(Seinfeld and Pandis, 2006).~~ aerosol aqueous phase chemistry. Under acidic conditions, SO₂ is mainly oxidized by transition
131 metal ions, while at pH > 5 the oxidation by O₃ and NO₂ predominates (Cheng et al., 2016). Therefore, the decrease of pH
132 during the last 50 years, even though being relatively modest, was sufficient to turn-off sulfate production from O₃ oxidation
133 (Fig. 5). At the same time, the increased aerosol acidity hinders the partitioning of nitric acid to the aerosol phase, reducing
134 the aerosol nitrate fraction from 90% to 80% (Fig. 3). Remarkably, the aerosol hygroscopicity has increased from ~0.3 in the
135 1970s to 0.45 recently (Fig. 4), revealing a reverse development compared to Europe and the USA. Here, the fraction of
136 mineral dust in the aerosol is higher; therefore, the particles gained hygroscopicity by the acquired pollution solutes.
137 Recently, the SO₂ emissions have dropped and the NO_x emission increase has slowed in East Asia, while SO₂ emissions are
138 soaring in South Asia. SO₂ emission trends since 2007 have been so drastic that inventories and scenarios tend to
139 ~~underestimate them overestimate the emitted SO₂~~. Satellite observations indicate that India has recently overtaken China as
140 the world largest emitter of SO₂ (Li et al., 2017). Following the satellite observations, we implemented the ~~large~~ significant
141 SO₂ reduction trends into our model (Fig. S2). Surprisingly, the effect only becomes noticeable over East Asia after 2016,
142 when the aerosol pH started increasing by about 0.3 units, while we do not find any change over South Asia. This
143 corroborates the strong buffering that we found over other regions such as Europe. Fig. 1 shows that NH₃ has been the major
144 buffer, supporting the recent findings of Zheng et al. (2020) that the acid-base pair of NH₄⁺/NH₃ provides the largest
145 buffering capacity over East and South Asia. However, we also found that in East Asia and to a lesser extent in South Asia
146 crustal elements, not considered in the study of Zheng et al. (2020), have contributed significantly on maintaining a mean pH
147 of 4.5 – 5 in the past decade (Fig. 1). ~~Calcium is the major crustal component of dust from the Gobi and Taklimakan deserts~~
148 ~~(Karydis et al., 2016) and unlike other crustal compounds it can react with sulfate ions and form insoluble CaSO₄, which~~
149 ~~precipitates out of the aerosol aqueous phase. This interaction reduces the aqueous sulfate and thus the aerosol acidity.~~

150 2.2.4 Tropical forests, Middle East

151 Over tropical forests, aerosols are typically not very acidic with pH values >4. Note that organic acids were not included in
152 the aerosol pH calculations, however, their contribution to the total ionic load is small (Andreae et al., 1988; Falkovich et al.,
153 2005), and aerosol acidity can be attributed to inorganic acids. Over the Amazon and Congo basins, the aerosol pH remained

154 around 5 since 1970. The Southeast Asian forest atmosphere is affected by pollution from mainland Asia, and the aerosol pH
155 decreased to around 4 recently. This pH drop has enhanced SOA formation from isoprene, since under low-NO_x conditions
156 (typical over rainforests) the presence of acidifying sulfate increases the reactive uptake of epoxydiols (Xu et al.,
157 2015;Surratt et al., 2010). Nevertheless, NH₃ emissions provide a remarkably strong buffer over all three tropical regions
158 while mineral dust cations are also important over the Amazon and Congo forests. Further, the Middle East is affected by
159 strong anthropogenic (fossil fuel related) and natural (aeolian dust) aerosol sources. Due to the high abundance of mineral
160 dust, the pH has remained close to 7. Without crustal cations, the pH would drop to about 4. Despite the omnipresence of
161 alkaline species from the surrounding deserts, NH₃ still plays a central role in controlling the acidification of mineral dust
162 aerosols, which can affect their hygroscopic growth and hence their climate forcing (Klingmüller et al., 2019;Klingmüller et
163 al., 2020).

164 2.2.5 Oceans

165 Over the Arctic and northern extra-tropical oceans, aerosol acidity is strongly affected by pollution transport from the urban-
166 industrial mid-latitudes. The Arctic aerosol pH is highly variable, remaining relatively low up to 1990 (~4.2), after which it
167 increased to about 5.2. Crustal cations are found to play a significant ~~buffering role~~ lowering the aerosol acidity. Over the
168 northern extra-tropical oceans, aerosol pH has remained relatively constant (~4.8). NH₃ provides an important alkaline
169 buffer, and without it the aerosol pH would have been below 3. NH₃ is also proved to be important over the tropical and
170 southern extra-tropical oceans, where a noticeable increase in aerosol acidity occurred after June 1991, when the eruption of
171 Mount Pinatubo in the Philippines released ~20 million tons of SO₂ into the stratosphere (McCormick et al., 1995). The
172 impact of Pinatubo sulfate, after returning to the troposphere, on aerosol acidity is mostly evident over Antarctica, where the
173 pH dropped by 2 units, as the stratospheric circulation is strongest in the winter hemisphere. Over Antarctica concentrations
174 of dust and especially of NH₃ are very low, and Fig. 1 illustrates that only in this pristine environment the large Pinatubo
175 anomaly could overwhelm the buffering by alkaline species. Except after Pinatubo, the pH has remained nearly constant at
176 5.8 over Antarctica and about 5.5 in the tropics and 6.8 in the southern extra-tropics.

177 3. Conclusions

178 We find that aerosol pH is generally well-buffered by alkaline compounds, notably NH₃ and in some areas crustal elements.
179 NH₃ is found to supply remarkable buffering capacity on a global scale, from the polluted continents to the remote oceans. In
180 the absence of NH₃, aerosols would be highly (to extremely) acidic in most of the world. Therefore, potential future changes
181 in NH₃ are critically important in this respect. Agriculture is the main NH₃ source and a controlling factor in fine particle
182 concentrations and health impacts in some areas (e.g., Europe) (Pozzer et al., 2017). The control of agricultural ammonia
183 emissions must therefore be accompanied by very strong reductions of SO₂ and NO_x to avoid that aerosols become highly

184 acidic with implications for human health (aerosol toxicity), ecosystems (acid deposition and nutrient availability), clouds
185 and climate (aerosol hygroscopicity).

186 4. Appendix A: Materials and Methods

187 4.1 Aerosol-chemistry-climate model

188 We used the ECHAM5/MESSy Atmospheric Chemistry (EMAC) model, which is a numerical chemistry and climate
189 simulation system that describes lower and middle atmosphere processes (Jöckel et al., 2006). EMAC uses the Modular
190 Earth Submodel System (MESSy2) (Jöckel et al., 2010) to link the different sub-models with an atmospheric dynamical core,
191 being an updated version of the 5th generation European Centre - Hamburg general circulation model (ECHAM5) (Roeckner
192 et al., 2006). EMAC has been extensively described and evaluated against in situ observations and satellite retrievals to
193 compute particulate matter concentrations and composition, aerosol optical depth, acid deposition, gas phase mixing ratios,
194 cloud properties, and meteorological parameters (Karydis et al., 2016; Pozzer et al., 2012; Tsimpidi et al., 2016; Karydis et al.,
195 2017; Bacer et al., 2018). The spectral resolution of EMAC used in this study is T63L31, corresponding to a horizontal grid
196 resolution of approximately $1.9^\circ \times 1.9^\circ$ and 31 vertical layers extending up to 10 hPa (i.e., 25 km) from the surface. The
197 presented model simulations encompass the 50-year period 1970-2020.

198 EMAC calculates fields of gas phase species online through the Module Efficiently Calculating the Chemistry of the
199 Atmosphere (MECCA) Submodel (Sander et al., 2019). MECCA calculates the concentration of a range of gases, including
200 aerosol precursor species (e.g. SO_2 , NH_3 , NO_x , DMS, H_2SO_4 and DMSO) and the major oxidant species (e.g. OH, H_2O_2 ,
201 NO_3 , and O_3). Aerosol microphysics are calculated by the Global Modal-aerosol eXtension (GMXe) module (Pringle et al.,
202 2010). The organic aerosol formation and atmospheric evolution are calculated by the ORACLE Submodel (Tsimpidi et al.,
203 2014, 2018). The aerosol size distribution is described by seven lognormal modes: four hydrophilic modes that cover the
204 aerosol size spectrum of nucleation, Aitken, accumulation and coarse modes, and three hydrophobic modes that cover the
205 same size range except nucleation. The aerosol composition within each size mode is uniform (internally mixed), however, it
206 varies between modes (externally mixed). Each mode is defined in terms of total number concentration, number mean radius,
207 and geometric standard deviation (Pringle et al., 2010). The removal of gas and aerosol species through wet and dry
208 deposition is calculated within the SCAV (Tost et al., 2006) and DRYDEP (Kerkweg et al., 2006) submodels, respectively.
209 The sedimentation of aerosols is calculated within the SEDI submodel (Kerkweg et al., 2006). The cloud cover,
210 microphysics and precipitation of large scale clouds is calculated by the CLOUD Submodel (Roeckner et al., 2006) which
211 uses a two-moment stratiform microphysical scheme (Lohmann and Ferrachat, 2010), and describes liquid droplet (Karydis
212 et al., 2017) and ice crystal (Bacer et al., 2018) formation by accounting for the aerosol physicochemical properties. The
213 effective hygroscopicity parameter κ is used to describe the influence of chemical composition on the cloud condensation
214 nuclei (CCN) activity of atmospheric aerosols. κ is calculated using the mixing rule of Petters and Kreidenweis (Petters and

215 Kreidenweis, 2007) and the individual κ parameter values for each inorganic salt (Petters and Kreidenweis, 2007; Sullivan et
216 al., 2009). Organic aerosol species are assumed to have a constant hygroscopicity κ parameter κ of 0.14 while bulk
217 mineral dust and black carbon are assumed to have zero hygroscopicity.

218 **4.2 Emissions**

219 The vertically distributed (Pozer et al., 2009) CMIP5 RCP8.5 emission inventory (van Vuuren et al., 2011) is used for the
220 anthropogenic and biomass burning emissions during the years 1970-2020. Direct emissions of aerosol components from
221 biofuel and open biomass burning are considered by using scaling factors applied on the emitted black carbon based on the
222 findings of Akagi et al. (Akagi et al., 2011) (Table S2). Dust emission fluxes and emissions of crustal species (Ca²⁺, Mg²⁺,
223 K⁺, Na⁺) are calculated online as described by Klingmuller, et al. (Klingmuller et al., 2018) and based on the chemical
224 composition of the emitted soil particles in every grid cell (Karydis et al., 2016); Table S3. NO_x produced by lightning is
225 calculated online and distributed vertically based on the parameterization of Grewe, et al. (Grewe et al., 2001). The
226 emissions of NO from soils are calculated online based on the algorithm of Yienger and Levy (Yienger and Levy, 1995). The
227 oceanic DMS emissions are calculated online by the AIRSEA Submodel (Pozer et al., 2006). The natural emissions of NH₃
228 are based on the GEIA database (Bouwman et al., 1997). Emissions of sea spray aerosols (assuming a composition suggested
229 by Seinfeld and Pandis (Seinfeld and Pandis, 2006); Table S2) and volcanic degassing emissions of SO₂ are based on the
230 offline emission data set of AEROCOM (Dentener et al., 2006).

231

232 **4.3 Thermodynamic model**

233 The inorganic aerosol composition, which is of prime importance for the accurate pH calculation, is computed with the
234 ISORROPIA-II thermodynamic equilibrium model (Fountoukis and Nenes, 2007). ISORROPIA-II calculates the
235 gas/liquid/solid equilibrium partitioning of the K⁺-Ca²⁺-Mg²⁺-NH₄⁺-Na⁺-SO₄²⁻-NO₃⁻-Cl-H₂O aerosol system and considers
236 the presence of 15 aqueous phase components and 19 salts in the solid phase. ISORROPIA-II solves for the equilibrium state
237 by considering the chemical potential of the species and minimizes the number of equations and iterations required by
238 considering specific compositional “regimes”. ~~Furthermore, to~~ The assumption of thermodynamic equilibrium is a good
239 approximation for fine-mode aerosols that rapidly reach equilibrium. However, the equilibrium timescale for large particles
240 is typically larger than the time step of the model (Meng and Seinfeld, 1996) leading to errors in the size distribution of
241 semi-volatile ions like nitrate. Since the current study include reactions of nitric acid with coarse sea-salt and dust aerosol
242 cations, the competition of fine and coarse particles for the available nitric acid can only be accurately represented by taking
243 into account the kinetic limitations during condensation of HNO₃ in the coarse mode aerosols. To account for kinetic
244 limitations by mass transfer and transport between the gas and particle phases, the process of gas/aerosol partitioning is
245 calculated in two stages (Pringle et al., 2010). First, the gaseous species that kinetically condense onto the aerosol phase

246 within the model timestep are calculated assuming diffusion limited condensation (Vignati et al., 2004). Then, ISORROPIA-
247 II re-distributes the mass between the gas and the aerosol phase assuming instant equilibrium between the two phases.

248 ISORROPIA-II is used in the forward mode, in which the total (i.e., gas and aerosol) concentrations are given as input.
249 Reverse mode calculations (i.e. when only the aerosol phase composition is known) should be avoided since they are
250 sensitive to errors and infer bimodal ~~behavior~~behaviour with highly acidic or highly alkaline particles, depending on whether
251 anions or cations are in excess (Song et al., 2018). While it is often assumed that aerosols are in a metastable state (i.e.,
252 composed only of a supersaturated aqueous phase), here we use ISORROPIA-II in the thermodynamically stable state mode
253 where salts are allowed to precipitate once the aqueous phase becomes saturated. For this purpose, we have used the revised
254 ISORROPIA-II model which includes modifications proposed by Song et al. (2018), who resolved coding errors related to
255 pH calculations when the stable state assumption is used. ~~A sensitivity simulation with only liquid aerosols (i.e., metastable)
256 revealed that the assumed particle phase state does not significantly impact the pH calculations over oceans and polluted
257 regions (e.g., Europe), however, the metastable assumption produces more acidic particles (up to 2 units of pH) in regions
258 affected by high concentrations of crustal cations (Fig. S3). Overall, the stable state assumption used here produces about 0.5
259 units higher global average pH than the metastable assumption.~~ By comparing with the benchmark thermodynamic model E-
260 AIM, Song et al. (2018) found that ISORROPIA-II produces somewhat higher pH (by 0.1-0.7 units, negatively correlated
261 with RH). However, E-AIM model versions either lack crustal cations from the ambient mixture of components (e.g. version
262 II) (Clegg et al., 1998), or only include Na⁺ with the restriction that it should be used when RH> 60% (e.g. version IV)
263 (Friese and Ebel, 2010). ~~Song et al. (2018) applied the revised ISORROPIA-II during winter haze events in eastern China
264 and found that the assumed particle phase state, either stable or metastable, does not significantly impact the pH predictions.~~

265 We performed a sensitivity simulation with only liquid aerosols (i.e., metastable), which revealed that the assumed
266 particle phase state does not significantly impact the pH calculations over oceans and polluted regions (e.g., Europe),
267 however, the metastable assumption produces more acidic particles (up to 2 units of pH) in regions affected by high
268 concentrations of crustal cations and consistently low RH values (Fig. S3). 4.3 Fountoukis et al. (2007) have shown that the
269 metastable solution predicts significant amounts of water below the mutual deliquescence relative humidity (MDRH, where
270 all salts are simultaneously saturated with respect to all components). Further, the generally high calcium concentrations
271 downwind of deserts results in increasing pH values due to the precipitation of insoluble salts such as the CaSO₄. The
272 metastable state assumption fails to reproduce this since it treats only the ions in the aqueous phase. In general, high amounts
273 of crustal species can significantly increase the aerosol pH which is consistent with the presence of excess carbonate in the
274 aerosol phase (Meng et al., 1995). It is worth mentioning that the stable state solution algorithm of ISORROPIA II starts
275 with assuming a dry aerosol, and based on the ambient RH dissolves each of the salts depending on their DRH. However, in
276 the ambient atmosphere, when the RH over a wet particle is decreasing, the wet aerosol may not crystallize below the
277 MDRH but instead remain in a metastable state affecting the uptake of water by the aerosol and thus the pH. This could be
278 the case in some locations with high diurnal variations of RH. Our sensitivity calculations show that, overall, the stable state
279 assumption produces an about 0.5 units higher global average pH than the metastable assumption. Karydis et al. (2016) have

280 shown that while the aerosol state assumption has a marginal effect on the calculated nitrate aerosol tropospheric burden (2%
281 change), it can be important over and downwind of deserts at very low RHs where nitrate is reduced by up to 60% by using
282 the metastable assumption. This is in accord with the findings of Ansari and Pandis (2000) who suggested that the stable
283 state results in higher concentrations of aerosol nitrate when the RH is low (<35 %) and/or sulfate to nitrate molar ratios are
284 low (<0.25).

285 **4.4 pH calculations**

286 The pH is defined as the negative decimal logarithm of the hydrogen ion activity ($a_{H^+} = \gamma x_{H^+}$) in a solution:

$$287 \text{pH} = -\log_{10}(\gamma x_{H^+})$$

$$288 \text{pH} = -\log_{10}(\gamma x_{H^+}) \quad (A1)$$

289 where x_{H^+} is the molality of hydrogen ions in the solution and γ is the ion activity coefficient of hydrogen. Assuming that γ
290 is unity, the aerosol pH can be calculated by using the hydrogen ion concentration in the aqueous aerosol phase calculated by
291 ISORROPIA-II (in mole m^{-3}) and the aerosol water content calculated by GMXe (in mole Kg^{-1}). GMXe assumes that particle
292 modes are internally mixed, and takes into account the contribution of both inorganic and organic (based on the organic
293 hygroscopicity parameter, $\kappa_{org} = 0.14$ ~~$\kappa = 0.14$~~ (Tsimpidi et al., 2014)) species to aerosol water.

294 The aerosol pH is calculated online at each timestep, and output stored every five hours based on instantaneous
295 concentrations of fine aerosol water and hydrogen ions. The average pH values shown in the manuscript are based on
296 the calculated instantaneous mean pH values. According to the Jensen's inequality (Jensen, 1906), the average of the
297 instantaneous pH values is less than or equal to the pH calculated based on the average of the water and hydrogen ion
298 instantaneous values. We estimate that the average pH calculated based on 5-hourly instantaneous values is approximately 1-
299 3 (~2 globally averaged) units higher than the pH calculated based on the average water and hydrogen ion concentrations. By
300 including online gas-particle partitioning calculations of the NH_3/HNO_3 system in polluted air, as applied here, we find that
301 the aerosol pH is higher by approximately one unit (Guo et al., 2015). Hence by neglecting these aspects the aerosol pH
302 would be low-biased by about 3 ~~points~~ units.

304 **4.5 Comparison against pH estimations from field derived $PM_{2.5}$ compositional data**

305 The pH calculated here is compared against pH estimations from field derived $PM_{2.5}$ compositional data around the
306 world compiled by Pye et al. (2020) (Table S1). pH data derived from other aerosol sizes (e.g., PM_{10}) has been omitted since
307 aerosol acidity can vary significantly with size (Zakoura et al., 2020). It should be emphasized that the comparison presented

308 in Table S1 aims to corroborate the spatial variability of pH found in this study and not to ~~strictly evaluate the model~~
309 ~~calculations. Observationally estimated aerosol pH is derived from a variety of methods that can affect the result~~
310 ~~significantly as discussed above (i.e., the use of E-AIM or ISORROPIA, stable/metastable assumption, forward/reverse~~
311 ~~mode, and the availability of gas-phase NH₃/HNO₃, crustal species, and organic aerosol-water observations).—evaluate the~~
312 ~~model calculations. Since direct measurements of aerosol acidity are not available, the observation-based aerosol pH is~~
313 ~~estimated by employing thermodynamic equilibrium models (e.g., ISORROPIA) and making assumptions that can~~
314 ~~significantly affect the results, especially when the data are averaged over extended periods, while RH conditions during data~~
315 ~~collection are not always accounted for, e.g. in studies based on filter sampling. The calculation of aerosol acidity on a global~~
316 ~~scale requires the advanced treatment of atmospheric aerosol chemical complexity, representing the real atmosphere, and~~
317 ~~beyond the conventional methods used by chemistry-climate models (CCM). The atmospheric chemistry model system~~
318 ~~EMAC is an ideal tool for this purpose since it is one of the most comprehensive CCM containing advanced descriptions of~~
319 ~~the aerosol thermodynamics (including e.g. dust-pollution interactions) and organic aerosol formation and atmospheric aging~~
320 ~~(affecting the aerosol water). Our model calculations for aerosol acidity are based on some processes/factors that are not~~
321 ~~included explicitly, usually neglected by model calculations used to constrain the aerosol acidity from observations. Sources~~
322 ~~of discrepancy between the pH calculations can be the following;~~

- 323 • ~~4-4The stable/metastable assumption does not affect the pH most of the time, however, in some cases with low RHs and~~
324 ~~the presence of crustal cations, the metastable assumption results in lower pHs (see section 4.3).~~
- 325 • ~~Crustal species from deserts and Na⁺ from sea salt can elevate the pH significantly in some locations, however, these~~
326 ~~are often neglected in observations.~~
- 327 • ~~The organic aerosols (which are treated comprehensively by our model using the module ORACLE and the volatility~~
328 ~~basis set framework (Tsimpidi et al., 2014)) can contribute significantly to the aerosol water, and thus increase the~~
329 ~~aerosol pH. This contribution is not considered by many observational studies.~~
- 330 • ~~Including gas phase species (e.g., NH₃, HNO₃) in the pH calculations is important. Using only the aerosol-phase as~~
331 ~~input (i.e., reverse mode) the inferred pH exhibits bimodal behaviour with very acidic or alkaline values depending on~~
332 ~~whether anions or cations are in excess (Hennigan et al., 2015). Even if the forward mode is used (without gas phase~~
333 ~~input), the calculated aerosol pH is biased low (approximately 1 pH unit) due to the repartition of semi-volatile anions~~
334 ~~(i.e., NH₃) to the gas phase to establish equilibrium (Guo et al., 2015).~~
- 335 • ~~Another important aspect, not explicitly mentioned in many studies, relates to the methods used to derive the campaign-~~
336 ~~average (or for 3D models the simulated average) pH. In our model the aerosol pH is calculated online (2-minute time~~
337 ~~resolution), while output is stored every five hours based on instantaneous concentrations of fine aerosol H₂O and H⁺.~~
338 ~~This mimics 5-hourly aerosol sampling. Then, the average pH values are calculated from the instantaneous mean pH~~
339 ~~values (see section 4.4). Often models use average values (and not instantaneous) as output, or field-derived pH~~
340 ~~calculations use average observed H₂O and H⁺ values, which can result in important underestimation (by ~ 1-3 units) of~~
341 ~~the aerosol pH (Jensen, 1906).~~

Formatted: English (United Kingdom)

- Some unrealistically high pH values in a few past studies resulted from coding errors in the stable state assumption of the ISORROPIA II model, which have been corrected in our study following the recommendation of Song et al. (2018).
- The type of thermodynamic model used is also important. Song et al. (2018) found that ISORROPIA-II produces somewhat higher pH (by 0.1-0.7 units, negatively correlated with RH) compared to the thermodynamic model E-AIM, which is used to observationally-constrain pH in some studies.
- Measurements of PM_{2.5} nitrate are not always reliable because of artifacts associated with the volatility of ammonium nitrate (Schaap et al., 2004). Ammonium and nitrate can partially evaporate from Teflon filters at temperatures between 15 to 20 °C and can evaporate completely at temperatures above. The evaporation from quartz filters is also significant at temperatures higher than 20 °C. This systematic underestimation of ammonium nitrate can affect the observed chemical composition of the aerosol and thus the pH calculations.
- The comparison between global model output and observations at specific locations. This also concerns the aerosol concentrations but is especially important for the aerosol acidity. Apart from the size of the model grid cells (i.e., ~ 1.9°x1.9°), the altitude is also important. The first vertical layer of EMAC is approximately 67m in height. On the other hand, ground observations are typically collected in a height up to 3 m. While the aerosols within size modes simulated in our model are well-mixed, perhaps this is not the case for the aerosols observed at the surface and potentially close to sources, and thus the aerosol acidity may be higher (e.g., due to the higher contribution from local primary sources like SO₄²⁻, lower water amounts in the aerosol, or lower concentrations of semi-volatile cations like NH₄⁺)

4.6 Emissions

The vertically distributed (Poizzer et al., 2009) CMIP5 RCP8.5 emission inventory (van Vuuren et al., 2011) is used for the anthropogenic and biomass burning emissions during the years 1970-2020. Direct emissions of aerosol components from biofuel and open biomass burning are considered by using scaling factors applied on the emitted black carbon based on the findings of Akagi, et al. (Akagi et al., 2011) (Table S2). Dust emission fluxes and emissions of crustal species (Ca²⁺, Mg²⁺, K⁺, Na⁺) are calculated online as described by Klingmuller, et al. (Klingmuller et al., 2018) and based on the chemical composition of the emitted soil particles in every grid cell (Karydis et al., 2016); Table S3. NO_x produced by lightning is calculated online and distributed vertically based on the parameterization of Grewe, et al. (Grewe et al., 2001). The emissions of NO from soils are calculated online based on the algorithm of Yienger and Levy (Yienger and Levy, 1995). The oceanic DMS emissions are calculated online by the AIRSEA Submodel (Poizzer et al., 2006). The natural emissions of NH₃ are based on the GEIA database (Bouwman et al., 1997). Emissions of sea spray aerosols (assuming a composition suggested by Seinfeld and Pandis (Seinfeld and Pandis, 2006); Table S2) and volcanic degassing emissions of SO₂ are based on the offline emission data set of AEROCOM (Dentener et al., 2006).

4.5 Partitioning of nitric acid between the gas and aerosol phases

The impact of pH on the fraction of nitrate in the particle phase relative to total nitrate (gas plus particle), i.e., $\varepsilon(\text{NO}_3^-)$, during the 50 years of simulation in specific regions is calculated as follows (Nah et al., 2018):

$$\varepsilon(\text{NO}_3^-) = \frac{H_{\text{HNO}_3}^* WRT (0.987 \times 10^{-14})}{\gamma_{\text{NO}_3^-} \gamma_{\text{H}^+} 10^{-\text{pH}} + H_{\text{HNO}_3}^* WRT (0.987 \times 10^{-14})} \quad (A2)$$

Where $H_{\text{HNO}_3}^*$ is the combined molality-based equilibrium constant of HNO_3 dissolution and deprotonation, γ 's represent the activity coefficients, W is the aerosol water, R is the gas constant, and T is the ambient temperature. Eq. A2 is equivalent with the instantaneous calculations of ISOROPIA II within EMAC. However, the model output is produced after considering all processes in the model and is not calculated at every timestep. Therefore, the use of Eq. 2 can provide a clearer picture of the impact of pH on HNO_3 gas/particle partitioning since the model output (e.g., gas-phase HNO_3 and nitrate in 4 size modes) is subject to uncertainties related to other processes (e.g., deposition, coagulation, transport, etc.).

4.6.7 Sulfate formation in aqueous aerosols

The sulfate production rate on aqueous aerosols from the heterogeneous oxidation of S(IV) with the dissolved O_3 is given by

$$R_o = k [\text{O}_3]_{\text{aq}} \quad (A3)$$

The first-order uptake rate, k , from monodisperse aerosols with radius r_a and total aerosol surface A , is calculated following Jacob (Jacob, 2000):

$$k = \left(\frac{r_a}{D_g} + \frac{4}{v\gamma} \right)^{-1} A \quad (A4)$$

where v is the mean molecular speed of O_3 and D_g is its gas-phase molecular diffusion coefficient calculated as follows:

$$D_g = \frac{9.45 \times 10^{17} \times \sqrt{T \left(3.47 \times 10^{-2} + \frac{1}{M} \right)}}{\rho_{\text{air}}} \quad (A5)$$

where T is the ambient air temperature, ρ_{air} is the air density, and M the molar mass of O_3 . γ is the reaction probability calculated following Jacob (Jacob, 2000) and Shao et al. (Shao et al., 2019).

$$\gamma = \left(\frac{1}{\alpha} + \frac{v}{4HRT \sqrt{D_a K f_r}} \right)^{-1} \quad (A6)$$

where α is the mass accommodation coefficient, D_a is the aqueous-phase molecular diffusion coefficient of O_3 , H is the effective Henry's law constant of O_3 (Sander, 2015), R is the ideal gas constant, f_r is the reacto-diffusive correction term (Shao et al., 2019), and K is the pseudo-first order reaction rate constant between S(IV) and O_3 in the aqueous phase (Seinfeld and Pandis, 2006).

Formatted: Font: Times New Roman

Formatted: Font: Cambria Math

400 5. References

- 401 [Abdelkader, M., Metzger, S., Mamouri, R. E., Astitha, M., Barrie, L., Levin, Z., and Lelieveld, J.: Dust-air pollution*](#)
402 [dynamics over the eastern Mediterranean, Atmospheric Chemistry and Physics, 15, 9173-9189, 10.5194/acp-15-9173-](#)
403 [2015, 2015.](#)
- 404 [Akagi, S. K., Yokelson, R. J., Wiedinmyer, C., Alvarado, M. J., Reid, J. S., Karl, T., Crounse, J. D., and Wennberg, P. O.:](#)
405 [Emission factors for open and domestic biomass burning for use in atmospheric models, Atmospheric Chemistry and](#)
406 [Physics, 11, 4039-4072, 10.5194/acp-11-4039-2011, 2011.](#)
- 407 [Andreae, M. O., Talbot, R. W., Andreae, T. W., and Harriss, R. C.: Formic and acetic acid over the central Amazon region,](#)
408 [Brazil. 1. dry season, Journal of Geophysical Research-Atmospheres, 93, 1616-1624, 10.1029/JD093iD02p01616, 1988.](#)
- 409 [Ansari, A. S., and Pandis, S. N.: The effect of metastable equilibrium states on the partitioning of nitrate between the gas and](#)
410 [aerosol phases, Atmospheric Environment, 34, 157-168, 10.1016/s1352-2310\(99\)00242-3, 2000.](#)
- 411 [Bacer, S., Sullivan, S. C., Karydis, V. A., Barahona, D., Kramer, M., Nenes, A., Tost, H., Tsimpidi, A. P., Lelieveld, J., and*](#)
412 [Pozer, A.: Implementation of a comprehensive ice crystal formation parameterization for cirrus and mixed-phase clouds](#)
413 [in the EMAC model \(based on MESSy 2.53\), Geoscientific Model Development, 11, 4021-4041, 10.5194/gmd-11-4021-](#)
414 [2018, 2018.](#)
- 415 [Behera, S. N., Betha, R., Liu, P., and Balasubramanian, R.: A study of diurnal variations of PM2.5 acidity and related](#)
416 [chemical species using a new thermodynamic equilibrium model, Science of The Total Environment, 452-453, 286-295,](#)
417 [https://doi.org/10.1016/j.scitotenv.2013.02.062, 2013.](#)
- 418 [Bouwman, A. F., Lee, D. S., Asman, W. A. H., Dentener, F. J., VanderHoek, K. W., and Olivier, J. G. J.: A global high-](#)
419 [resolution emission inventory for ammonia, Global Biogeochemical Cycles, 11, 561-587, 10.1029/97gb02266, 1997.](#)
- 420 [Cheng, Y. F., Zheng, G. J., Wei, C., Mu, Q., Zheng, B., Wang, Z. B., Gao, M., Zhang, Q., He, K. B., Carmichael, G., Poschl,](#)
421 [U., and Su, H.: Reactive nitrogen chemistry in aerosol water as a source of sulfate during haze events in China, Science](#)
422 [Advances, 2, 10.1126/sciadv.1601530, 2016.](#)
- 423 [Clegg, S. L., Brimblecombe, P., and Wexler, A. S.: Thermodynamic model of the system H+-NH4+-Na+-SO4--NB3--Cl-](#)
424 [H2O at 298.15 K, J. Phys. Chem. A, 102, 2155-2171, 10.1021/jp973043j, 1998.](#)
- 425 [Dall'Osto, M., Ains, R. L., Beale, R., Cree, C., Fitzsimons, M. F., Beddows, D., Harrison, R. M., Ceburnis, D., O'Dowd, C.,](#)
426 [Rinaldi, M., Paglione, M., Nenes, A., Decesari, S., and Simó, R.: Simultaneous Detection of Alkylamines in the Surface](#)
427 [Ocean and Atmosphere of the Antarctic Sympagic Environment, ACS Earth and Space Chemistry, 3, 854-862,](#)
428 [10.1021/acsearthspacechem.9b00028, 2019.](#)
- 429 [Dentener, F., Kinne, S., Bond, T., Boucher, O., Cofala, J., Generoso, S., Ginoux, P., Gong, S., Hoelzemann, J. J., Ito, A.,](#)
430 [Marelli, L., Penner, J. E., Putaud, J. P., Textor, C., Schulz, M., van der Werf, G. R., and Wilson, J.: Emissions of primary](#)
431 [aerosol and precursor gases in the years 2000 and 1750 prescribed data-sets for AeroCom, Atmos. Chem. Phys., 6, 4321-](#)
432 [4344, 2006.](#)
- 433 [Falkovich, A. H., Graber, E. R., Schkolnik, G., Rudich, Y., Maenhaut, W., and Artaxo, P.: Low molecular weight organic](#)
434 [acids in aerosol particles from Rondonia, Brazil, during the biomass-burning, transition and wet periods, Atmospheric](#)
435 [Chemistry and Physics, 5, 781-797, 10.5194/acp-5-781-2005, 2005.](#)
- 436 [Fang, T., Guo, H. Y., Zeng, L. H., Verma, V., Nenes, A., and Weber, R. J.: Highly Acidic Ambient Particles, Soluble](#)
437 [Metals, and Oxidative Potential: A Link between Sulfate and Aerosol Toxicity, Environmental Science & Technology,](#)
438 [51, 2611-2620, 10.1021/acs.est.6b06151, 2017.](#)
- 439 [Fountoukis, C., and Nenes, A.: ISORROPIA II: a computationally efficient thermodynamic equilibrium model for K+-Ca2+-](#)
440 [Mg2+-NH4+-Na+-SO42--NO3--Cl-H2O aerosols, Atmospheric Chemistry and Physics, 7, 4639-4659, 2007.](#)
- 441 [Friese, E., and Ebel, A.: Temperature Dependent Thermodynamic Model of the System](#)
442 [H+-NH4+-Na+-SO42--NO3--Cl--H2O, The Journal of Physical Chemistry A, 114, 11595-11631,](#)
443 [10.1021/jp101041j, 2010.](#)
- 444 [Grewé, V., Brunner, D., Dameris, M., Grenfell, J. L., Hein, R., Shindell, D., and Staehelin, J.: Origin and variability of upper](#)
445 [tropospheric nitrogen oxides and ozone at northern mid-latitudes, Atmospheric Environment, 35, 3421-3433,](#)
446 [10.1016/s1352-2310\(01\)00134-0, 2001.](#)

Formatted: Font: +Body (Times New Roman), 10 pt, English (United States)

Formatted: Indent: Left: 0 cm, Hanging: 0.5 cm

Formatted: Font: +Body (Times New Roman), 10 pt, English (United States)

Formatted: Indent: Left: 0 cm, Hanging: 0.5 cm

Formatted: Font: +Body (Times New Roman), 10 pt, English (United States)

447 Guo, H., Xu, L., Bougiatioti, A., Cerully, K. M., Capps, S. L., Hite, J. R., Carlton, A. G., Lee, S. H., Bergin, M. H., Ng, N.
448 L., Nenes, A., and Weber, R. J.: Fine-particle water and pH in the southeastern United States, *Atmospheric Chemistry
449 and Physics*, 15, 5211-5228, 10.5194/acp-15-5211-2015, 2015.

450 Guo, H., Sullivan, A. P., Campuzano-Jost, P., Schroder, J. C., Lopez-Hilfiker, F. D., Dibb, J. E., Jimenez, J. L., Thornton, J.
451 A., Brown, S. S., Nenes, A., and Weber, R. J.: Fine particle pH and the partitioning of nitric acid during winter in the
452 northeastern United States, *Journal of Geophysical Research-Atmospheres*, 121, 10355-10376, 10.1002/2016jd025311,
453 2016.

454 Guo, H., Otjes, R., Schlag, P., Kiendler-Scharr, A., Nenes, A., and Weber, R. J.: Effectiveness of ammonia reduction on
455 control of fine particle nitrate, *Atmospheric Chemistry and Physics*, 18, 12241-12256, 10.5194/acp-18-12241-2018,
456 2018.

457 Guo, H. Y., Liu, J. M., Froyd, K. D., Roberts, J. M., Veres, P. R., Hayes, P. L., Jimenez, J. L., Nenes, A., and Weber, R. J.:
458 Fine particle pH and gas-particle phase partitioning of inorganic species in Pasadena, California, during the 2010 CalNex
459 campaign, *Atmospheric Chemistry and Physics*, 17, 5703-5719, 10.5194/acp-17-5703-2017, 2017.

460 Hennigan, C. J., Izumi, J., Sullivan, A. P., Weber, R. J., and Nenes, A.: A critical evaluation of proxy methods used to
461 estimate the acidity of atmospheric particles, *Atmospheric Chemistry and Physics*, 15, 2775-2790, 10.5194/acp-15-2775-
462 2015, 2015.

463 Jacob, D. J.: Heterogeneous chemistry and tropospheric ozone, *Atmospheric Environment*, 34, 2131-2159, 10.1016/s1352-
464 2310(99)00462-8, 2000.

465 Jensen, J.: On the convex functions and inequalities between mean values, *Acta Mathematica*, 30, 175-193,
466 10.1007/bf02418571, 1906.

467 Jia, S., Wang, X., Zhang, Q., Sarkar, S., Wu, L., Huang, M., Zhang, J., and Yang, L.: Technical note: Comparison and
468 interconversion of pH based on different standard states for aerosol acidity characterization, *Atmos. Chem. Phys.*, 18,
469 11125-11133, 10.5194/acp-18-11125-2018, 2018.

470 Jickells, T. D., An, Z. S., Andersen, K. K., Baker, A. R., Bergametti, G., Brooks, N., Cao, J. J., Boyd, P. W., Duce, R. A.,
471 Hunter, K. A., Kawahata, H., Kubilay, N., laRoche, J., Liss, P. S., Mahowald, N., Prospero, J. M., Ridgwell, A. J., Tegen,
472 I., and Torres, R.: Global iron connections between desert dust, ocean biogeochemistry, and climate, *Science*, 308, 67-71,
473 10.1126/science.1105959, 2005.

474 Jöckel, P., Tost, H., Pozzer, A., Bruehl, C., Buchholz, J., Ganzeveld, L., Hoor, P., Kerkweg, A., Lawrence, M. G., Sander,
475 R., Steil, B., Stiller, G., Tanarhte, M., Taraborrelli, D., Van Aardenne, J., and Lelieveld, J.: The atmospheric chemistry
476 general circulation model ECHAM5/MESSy1: consistent simulation of ozone from the surface to the mesosphere,
477 *Atmos. Chem. Phys.*, 6, 5067-5104, 2006.

478 Jöckel, P., Kerkweg, A., Pozzer, A., Sander, R., Tost, H., Riede, H., Baumgaertner, A., Gromov, S., and Kern, B.:
479 Development cycle 2 of the Modular Earth Submodel System (MESSy2), *Geoscientific Model Development*, 3, 717-752,
480 2010.

481 Karydis, V. A., Tsimpidi, A. P., Pozzer, A., Astitha, M., and Lelieveld, J.: Effects of mineral dust on global atmospheric
482 nitrate concentrations, *Atmos. Chem. Phys.*, 16, 1491-1509, 10.5194/acp-16-1491-2016, 2016.

483 Karydis, V. A., Tsimpidi, A. P., Bacer, S., Pozzer, A., Nenes, A., and Lelieveld, J.: Global impact of mineral dust on cloud
484 droplet number concentration, *Atmospheric Chemistry and Physics*, 17, 5601-5621, 10.5194/acp-17-5601-2017, 2017.

485 Kerkweg, A., Buchholz, J., Ganzeveld, L., Pozzer, A., Tost, H., and Jöckel, P.: Technical Note: An implementation of the
486 dry removal processes DRY DEPosition and SEDimentation in the Modular Earth Submodel System (MESSy), *Atmos.*
487 *Chem. Phys.*, 6, 4617-4632, 2006.

488 Klingmüller, K., Metzger, S., Abdelkader, M., Karydis, V. A., Stenchikov, G. L., Pozzer, A., and Lelieveld, J.: Revised
489 mineral dust emissions in the atmospheric chemistry-climate model EMAC (MESSy 2.52 DU_Astithal KKDU2017
490 patch), *Geoscientific Model Development*, 11, 989-1008, 10.5194/gmd-11-989-2018, 2018.

491 Klingmüller, K., Lelieveld, J., Karydis, V. A., and Stenchikov, G. L.: Direct radiative effect of dust-pollution interactions,
492 *Atmospheric Chemistry and Physics*, 19, 7397-7408, 10.5194/acp-19-7397-2019, 2019.

493 Klingmüller, K., Karydis, V. A., Bacer, S., Stenchikov, G. L., and Lelieveld, J.: Weaker cooling by aerosols due to dust-
494 pollution interactions, *Atmos. Chem. Phys. Discuss.*, 2020, 1-19, 10.5194/acp-2020-531, 2020.

495 Lawal, A. S., Guan, X. B., Liu, C., Henneman, L. R. F., Vasilakos, P., Bhogineni, V., Weber, R. J., Nenes, A., and Russell,
496 A. G.: Linked Response of Aerosol Acidity and Ammonia to SO₂ and NO_x Emissions Reductions in the United States,
497 Environmental Science & Technology, 52, 9861-9873, 10.1021/acs.est.8b00711, 2018.

498 Lelieveld, J., Evans, J. S., Fnais, M., Giannadaki, D., and Pozzer, A.: The contribution of outdoor air pollution sources to
499 premature mortality on a global scale, Nature, 525, 367-371, 10.1038/nature15371, 2015.

500 Leygraf, C., Wallinder, I. O., Tidblad, J., and Graedel, T.: Atmospheric Corrosion, John Wiley & Sons, 2016.

501 Li, C., McLinden, C., Fioletov, V., Krotkov, N., Carn, S., Joiner, J., Streets, D., He, H., Ren, X., Li, Z., and Dickerson, R. R.:
502 India Is Overtaking China as the World's Largest Emitter of Anthropogenic Sulfur Dioxide, Scientific Reports, 7, 14304,
503 10.1038/s41598-017-14639-8, 2017.

504 Lohmann, U., and Ferrachat, S.: Impact of parametric uncertainties on the present-day climate and on the anthropogenic
505 aerosol effect, Atmos. Chem. Phys., 10, 11373-11383, 10.5194/acp-10-11373-2010, 2010.

506 Marais, E. A., Jacob, D. J., Jimenez, J. L., Campuzano-Jost, P., Day, D. A., Hu, W., Krechmer, J., Zhu, L., Kim, P. S.,
507 Miller, C. C., Fisher, J. A., Travis, K., Yu, K., Hanisco, T. F., Wolfe, G. M., Arkinson, H. L., Pye, H. O. T., Froyd, K. D.,
508 Liao, J., and McNeill, V. F.: Aqueous-phase mechanism for secondary organic aerosol formation from isoprene:
509 application to the southeast United States and co-benefit of SO₂ emission controls, Atmospheric Chemistry and Physics,
510 16, 1603-1618, 10.5194/acp-16-1603-2016, 2016.

511 Masiol, M., Squizzato, S., Formenton, G., Khan, M. B., Hopke, P. K., Nenes, A., Pandis, S. N., Tositti, L., Benetello, F.,
512 Visin, F., and Pavoni, B.: Hybrid multiple-site mass closure and source apportionment of PM_{2.5} and aerosol acidity at
513 major cities in the Po Valley, Science of The Total Environment, 704, 135287,
514 <https://doi.org/10.1016/j.scitotenv.2019.135287>, 2020.

515 McCormick, M. P., Thomason, L. W., and Trepte, C. R.: ATMOSPHERIC EFFECTS OF THE MT-PINATUBO
516 ERUPTION, Nature, 373, 399-404, 10.1038/373399a0, 1995.

517 [Meng, Z. Y., Seinfeld, J. H., Saxena, P., and Kim, Y. P.: Atmospheric gas-aerosol equilibrium .4. Thermodynamics of
518 carbonates, Aerosol Science and Technology, 23, 131-154, 1995.](#)

519 [Meng, Z. Y., and Seinfeld, J. H.: Time scales to achieve atmospheric gas-aerosol equilibrium for volatile species,
520 Atmospheric Environment, 30, 2889-2900, 10.1016/1352-2310\(95\)00493-9, 1996.](#)

521 Metzger, S., Mihalopoulos, N., and Lelieveld, J.: Importance of mineral cations and organics in gas-aerosol partitioning of
522 reactive nitrogen compounds: case study based on MINOS results, Atmospheric Chemistry and Physics, 6, 2549-2567,
523 10.5194/acp-6-2549-2006, 2006.

524 Nah, T., Guo, H., Sullivan, A. P., Chen, Y., Tanner, D. J., Nenes, A., Russell, A., Ng, N. L., Huey, L. G., and Weber, R. J.:
525 Characterization of aerosol composition, aerosol acidity, and organic acid partitioning at an agriculturally intensive rural
526 southeastern US site, Atmos. Chem. Phys., 18, 11471-11491, 10.5194/acp-18-11471-2018, 2018.

527 Nenes, A., Pandis, S. N., Weber, R. J., and Russell, A.: Aerosol pH and liquid water content determine when particulate
528 matter is sensitive to ammonia and nitrate availability, Atmospheric Chemistry and Physics, 20, 3249-3258, 10.5194/acp-
529 20-3249-2020, 2020.

530 Oakes, M., Ingall, E. D., Lai, B., Shafer, M. M., Hays, M. D., Liu, Z. G., Russell, A. G., and Weber, R. J.: Iron Solubility
531 Related to Particle Sulfur Content in Source Emission and Ambient Fine Particles, Environmental Science &
532 Technology, 46, 6637-6644, 10.1021/es300701c, 2012.

533 Park, M., Joo, H. S., Lee, K., Jang, M., Kim, S. D., Kim, I., Borlaza, L. J. S., Lim, H., Shin, H., Chung, K. H., Choi, Y.-H.,
534 Park, S. G., Bae, M.-S., Lee, J., Song, H., and Park, K.: Differential toxicities of fine particulate matters from various
535 sources, Scientific Reports, 8, 17007, 10.1038/s41598-018-35398-0, 2018.

536 Pathak, R. K., Yao, X. H., and Chan, C. K.: Sampling artifacts of acidity and ionic species in PM_{2.5}, Environmental Science
537 & Technology, 38, 254-259, 10.1021/es0342244, 2004.

538 Pathak, R. K., Wu, W. S., and Wang, T.: Summertime PM_{2.5} ionic species in four major cities of China: nitrate
539 formation in an ammonia-deficient atmosphere, Atmos. Chem. Phys., 9, 1711-1722, 10.5194/acp-9-1711-2009, 2009.

540 Petters, M. D., and Kreidenweis, S. M.: A single parameter representation of hygroscopic growth and cloud condensation
541 nucleus activity, Atmospheric Chemistry and Physics, 7, 1961-1971, 2007.

542 Pozzer, A., Joeckel, P. J., Sander, R., Williams, J., Ganzeveld, L., and Lelieveld, J.: Technical note: the MESSY-submodel
543 AIRSEA calculating the air-sea exchange of chemical species, Atmos. Chem. Phys., 6, 5435-5444, 2006.

Formatted: Font: +Body (Times New Roman), 10 pt, English (United States)

Formatted: Font: +Body (Times New Roman), 10 pt, English (United States)

Formatted: Indent: Left: 0 cm, Hanging: 0.5 cm

544 Pozzer, A., Jockel, P., and Van Aardenne, J.: The influence of the vertical distribution of emissions on tropospheric
545 chemistry, *Atmospheric Chemistry and Physics*, 9, 9417-9432, 2009.

546 Pozzer, A., de Meij, A., Pringle, K. J., Tost, H., Doering, U. M., van Aardenne, J., and Lelieveld, J.: Distributions and
547 regional budgets of aerosols and their precursors simulated with the EMAC chemistry-climate model, *Atmos. Chem.*
548 *Phys.*, 12, 961-987, 2012.

549 Pozzer, A., Tsimpidi, A. P., Karydis, V. A., de Meij, A., and Lelieveld, J.: Impact of agricultural emission reductions on
550 fine-particulate matter and public health, *Atmospheric Chemistry and Physics*, 17, 12813-12826, 10.5194/acp-17-12813-
551 2017, 2017.

552 Pringle, K. J., Tost, H., Message, S., Steil, B., Giannadaki, D., Nenes, A., Fountoukis, C., Stier, P., Vignati, E., and Lelieveld, J.:
553 Description and evaluation of GMXe: a new aerosol submodel for global simulations (v1), *Geoscientific Model*
554 *Development*, 3, 391-412, 2010.

555 Pye, H. O. T., Nenes, A., Alexander, B., Ault, A. P., Barth, M. C., Clegg, S. L., Collett, J. L., Fahey, K. M., Hennigan, C. J.,
556 Herrmann, H., Kanakidou, M., Kelly, J. T., Ku, I. T., McNeill, V. F., Riemer, N., Schaefer, T., Shi, G. L., Tilgner, A.,
557 Walker, J. T., Wang, T., Weber, R., Xing, J., Zaveri, R. A., and Zuend, A.: The acidity of atmospheric particles and
558 clouds, *Atmospheric Chemistry and Physics*, 20, 4809-4888, 10.5194/acp-20-4809-2020, 2020.

559 Raizenne, M., Neas, L. M., Damokosh, A. I., Dockery, D. W., Spengler, J. D., Koutrakis, P., Ware, J. H., and Speizer, F. E.:
560 Health effects of acid aerosols on North American children: Pulmonary function, *Environmental Health Perspectives*,
561 104, 506-514, 10.2307/3432991, 1996.

562 Roeckner, E., Brokopf, R., Esch, M., Giorgetta, M., Hagemann, S., Kornblueh, L., Manzini, E., Schlese, U., and
563 Schulzweida, U.: Sensitivity of simulated climate to horizontal and vertical resolution in the ECHAM5 atmosphere
564 model, *Journal of Climate*, 19, 3771-3791, 10.1175/jcli3824.1, 2006.

565 Saiz-Lopez, A., and von Glasow, R.: Reactive halogen chemistry in the troposphere, *Chemical Society Reviews*, 41, 6448-
566 6472, 10.1039/c2cs35208g, 2012.

567 Sander, R.: Compilation of Henry's law constants (version 4.0) for water as solvent, *Atmos. Chem. Phys.*, 15, 4399-4981,
568 10.5194/acp-15-4399-2015, 2015.

569 Sander, R., Baumgaertner, A., Cabrera-Perez, D., Frank, F., Gromov, S., Grooss, J. U., Harder, H., Huijnen, V., Jockel, P.,
570 Karydis, V. A., Niemeyer, K. E., Pozzer, A., Hella, R. B., Schultz, M. G., Taraborrelli, D., and Tauer, S.: The community
571 atmospheric chemistry box model CAABA/MECCA-4.0, *Geoscientific Model Development*, 12, 1365-1385,
572 10.5194/gmd-12-1365-2019, 2019.

573 [Schaap, M., van Loon, M., ten Brink, H. M., Dentener, F. J., and Buitjes, P. J. H.: Secondary inorganic aerosol simulations
574 for Europe with special attention to nitrate, *Atmos. Chem. Phys.*, 4, 857-874, 10.5194/acp-4-857-2004, 2004.](#)

575 Seinfeld, J. H., and Pandis, S. N.: *Atmospheric Chemistry and Physics: From Air Pollution to Climate Change*, Second ed.,
576 John Wiley & Sons, Inc., Hoboken, New Jersey, 2006.

577 Shao, J., Chen, Q., Wang, Y., Lu, X., He, P., Sun, Y., Shah, V., Martin, R. V., Philip, S., Song, S., Zhao, Y., Xie, Z., Zhang,
578 L., and Alexander, B.: Heterogeneous sulfate aerosol formation mechanisms during wintertime Chinese haze events: air
579 quality model assessment using observations of sulfate oxygen isotopes in Beijing, *Atmos. Chem. Phys.*, 19, 6107-6123,
580 10.5194/acp-19-6107-2019, 2019.

581 Shi, G., Xu, J., Peng, X., Xiao, Z., Chen, K., Tian, Y., Guan, X., Feng, Y., Yu, H., Nenes, A., and Russell, A. G.: pH of
582 Aerosols in a Polluted Atmosphere: Source Contributions to Highly Acidic Aerosol, *Environmental Science &*
583 *Technology*, 51, 4289-4296, 10.1021/acs.est.6b05736, 2017.

584 Song, S., Gao, M., Xu, W., Shao, J., Shi, G., Wang, S., Wang, Y., Sun, Y., and McElroy, M. B.: Fine-particle pH for Beijing
585 winter haze as inferred from different thermodynamic equilibrium models, *Atmos. Chem. Phys.*, 18, 7423-7438,
586 10.5194/acp-18-7423-2018, 2018.

587 Squizzato, S., Masiol, M., Brunelli, A., Pistollato, S., Tarabotti, E., Rampazzo, G., and Pavoni, B.: Factors determining the
588 formation of secondary inorganic aerosol: a case study in the Po Valley (Italy), *Atmos. Chem. Phys.*, 13, 1927-1939,
589 10.5194/acp-13-1927-2013, 2013.

590 Sullivan, R. C., Moore, M. J. K., Petters, M. D., Kreidenweis, S. M., Roberts, G. C., and Prather, K. A.: Effect of chemical
591 mixing state on the hygroscopicity and cloud nucleation properties of calcium mineral dust particles, *Atmospheric*
592 *Chemistry and Physics*, 9, 3303-3316, 2009.

Formatted: Font: +Body (Times New Roman), 10 pt, English (United States)

Formatted: Indent: Left: 0 cm, Hanging: 0.5 cm

593 Surratt, J. D., Chan, A. W. H., Eddingsaas, N. C., Chan, M. N., Loza, C. L., Kwan, A. J., Hersey, S. P., Flagan, R. C.,
594 Wennberg, P. O., and Seinfeld, J. H.: Reactive intermediates revealed in secondary organic aerosol formation from
595 isoprene, *Proceedings of the National Academy of Sciences of the United States of America*, 107, 6640-6645,
596 10.1073/pnas.091114107, 2010.

597 Tan, T., Hu, M., Li, M., Guo, Q., Wu, Y., Fang, X., Gu, F., Wang, Y., and Wu, Z.: New insight into PM_{2.5} pollution
598 patterns in Beijing based on one-year measurement of chemical compositions, *Science of The Total Environment*, 621,
599 734-743, <https://doi.org/10.1016/j.scitotenv.2017.11.208>, 2018.

600 Tost, H., Jockel, P. J., Kerkweg, A., Sander, R., and Lelieveld, J.: Technical note: A new comprehensive SCAVenging
601 submodel for global atmospheric chemistry modelling, *Atmos. Chem. Phys.*, 6, 565-574, 2006.

602 Tsimpidi, A. P., Karydis, V. A., Pozzer, A., Pandis, S. N., and Lelieveld, J.: ORACLE (v1.0): module to simulate the organic
603 aerosol composition and evolution in the atmosphere, *Geoscientific Model Development*, 7, 3153-3172, 10.5194/gmd-7-
604 3153-2014, 2014.

605 Tsimpidi, A. P., Karydis, V. A., Pandis, S. N., and Lelieveld, J.: Global combustion sources of organic aerosols: model
606 comparison with 84 AMS factor-analysis data sets, *Atmos. Chem. Phys.*, 16, 8939-8962, 10.5194/acp-16-8939-2016,
607 2016.

608 Tsimpidi, A. P., Karydis, V. A., Pozzer, A., Pandis, S. N., and Lelieveld, J.: ORACLE 2-D (v2.0): an efficient module to
609 compute the volatility and oxygen content of organic aerosol with a global chemistry-climate model, *Geoscientific Model*
610 *Development*, 11, 3369-3389, 10.5194/gmd-11-3369-2018, 2018.

611 van Vuuren, D. P., Edmonds, J., Kainuma, M., Riahi, K., Thomson, A., Hibbard, K., Hurtt, G. C., Kram, T., Krey, V.,
612 Lamarque, J. F., Masui, T., Meinshausen, M., Nakicenovic, N., Smith, S. J., and Rose, S. K.: The representative
613 concentration pathways: an overview, *Climatic Change*, 109, 5-31, 10.1007/s10584-011-0148-z, 2011.

614 Vieira-Filho, M., Pedrotti, J. J., and Fornaro, A.: Water-soluble ions species of size-resolved aerosols: Implications for the
615 atmospheric acidity in São Paulo megacity, Brazil, *Atmospheric Research*, 181, 281-287,
616 <https://doi.org/10.1016/j.atmosres.2016.07.006>, 2016.

617 Vignati, E., Wilson, J., and Stier, P.: M7: An efficient size-resolved aerosol microphysics module for large-scale aerosol
618 transport models, *J. Geophys. Res.-Atmos.*, 109, doi: 10.1029/2003jd004485, 2004.

619 Wang, H., Ding, J., Xu, J., Wen, J., Han, J., Wang, K., Shi, G., Feng, Y., Ivey, C. E., Wang, Y., Nenes, A., Zhao, Q., and
620 Russell, A. G.: Aerosols in an arid environment: The role of aerosol water content, particulate acidity, precursors, and
621 relative humidity on secondary inorganic aerosols, *Science of The Total Environment*, 646, 564-572,
622 <https://doi.org/10.1016/j.scitotenv.2018.07.321>, 2019a.

623 Wang, Y., Li, W., Gao, W., Liu, Z., Tian, S., Shen, R., Ji, D., Wang, S., Wang, L., Tang, G., Song, T., Cheng, M., Wang, G.,
624 Gong, Z., Hao, J., and Zhang, Y.: Trends in particulate matter and its chemical compositions in China from 2013–2017,
625 *Science China Earth Sciences*, 62, 1857-1871, 10.1007/s11430-018-9373-1, 2019b.

626 Weber, R. J., Guo, H. Y., Russell, A. G., and Nenes, A.: High aerosol acidity despite declining atmospheric sulfate
627 concentrations over the past 15 years, *Nature Geoscience*, 9, 282-285, 10.1038/ngeo2665, 2016.

628 Xu, L., Guo, H. Y., Boyd, C. M., Klein, M., Bougiatioti, A., Cerully, K. M., Hite, J. R., Isaacman-VanWertz, G., Kreisberg,
629 N. M., Knote, C., Olson, K., Koss, A., Goldstein, A. H., Hering, S. V., de Gouw, J., Baumann, K., Lee, S. H., Nenes, A.,
630 Weber, R. J., and Ng, N. L.: Effects of anthropogenic emissions on aerosol formation from isoprene and monoterpenes in
631 the southeastern United States, *Proceedings of the National Academy of Sciences of the United States of America*, 112,
632 37-42, 10.1073/pnas.1417609112, 2015.

633 Xue, J., Lau, A. K. H., and Yu, J. Z.: A study of acidity on PM_{2.5} in Hong Kong using online ionic chemical composition
634 measurements, *Atmospheric Environment*, 45, 7081-7088, <https://doi.org/10.1016/j.atmosenv.2011.09.040>, 2011.

635 Yao, X., Ling, T. Y., Fang, M., and Chan, C. K.: Size dependence of in situ pH in submicron atmospheric particles in Hong
636 Kong, *Atmospheric Environment*, 41, 382-393, <https://doi.org/10.1016/j.atmosenv.2006.07.037>, 2007.

637 Yienger, J. J., and Levy, H.: Empirical-model of global soil-biogenic NO_x emissions, *Journal of Geophysical Research-*
638 *Atmospheres*, 100, 11447-11464, 10.1029/95jd00370, 1995.

639 Zakoura, M., Kakavas, S., Nenes, A., and Pandis, S. N.: Size-resolved aerosol pH over Europe during summer, *Atmos.*
640 *Chem. Phys. Discuss.*, 2020, 1-24, 10.5194/acp-2019-1146, 2020.

641 Zheng, G., Su, H., Wang, S., Andreae, M. O., Pöschl, U., and Cheng, Y.: Multiphase buffer theory explains contrasts in
642 atmospheric aerosol acidity, *Science*, 369, 1374-1377, 10.1126/science.aba3719, 2020.

Formatted: Font: +Body (Times New Roman), 10 pt, English (United States)

Formatted: Font: +Body (Times New Roman), 10 pt, English (United States)

Formatted: Font: +Body (Times New Roman), 10 pt, English (United States)

Formatted: Font: +Body (Times New Roman), 10 pt, English (United States)

Formatted: Font: +Body (Times New Roman), 10 pt, English (United States)

Formatted: English (United States)

643

644

645 **Author contributions:** V.A.K. and J.L. planned the research, V.A.K., A.P.T. and A.P. performed the model calculations,

646 V.A.K., A.P., and J.L. analyzed the results, V.A.K. and J.L. wrote the paper. All authors contributed to the manuscript.:

647 **Competing interests:** Authors declare no competing interests. **Code/Data availability:** Data and related material can be

648 obtained from V.A.K. (v.karydis@fz-juelich.de) upon request.

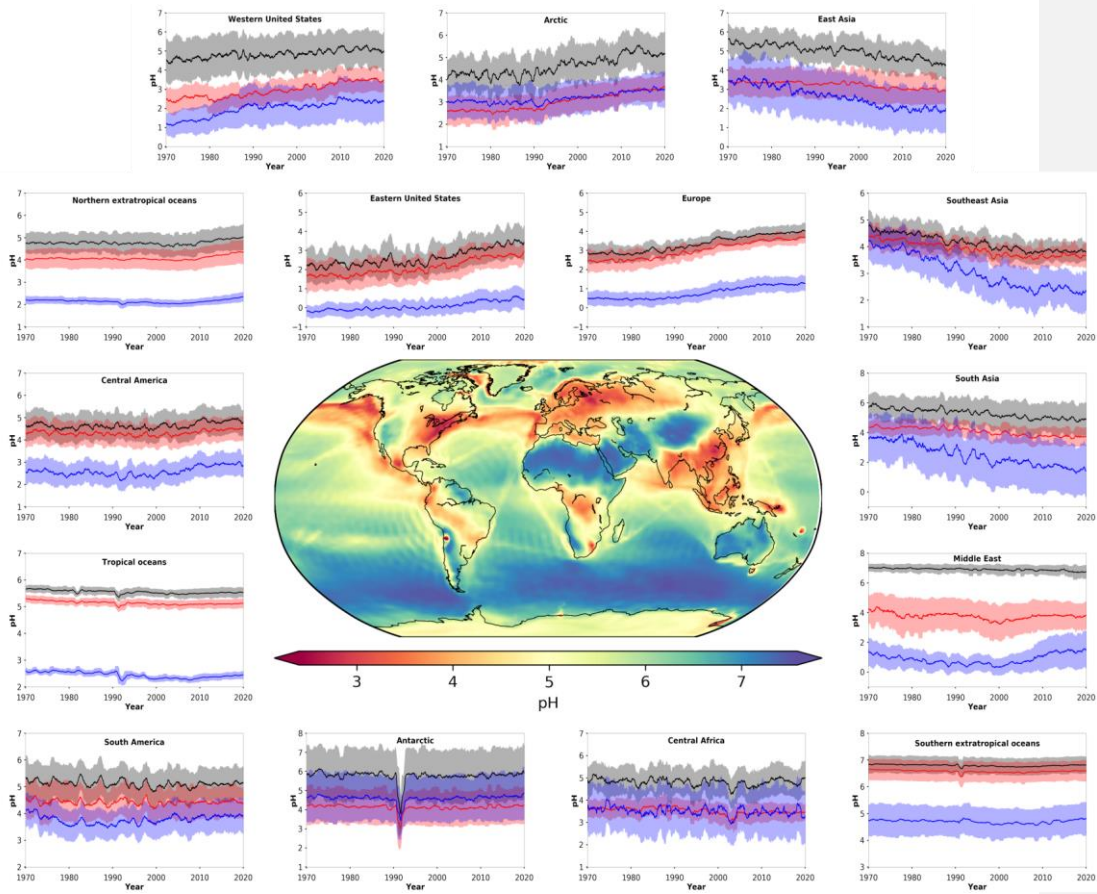
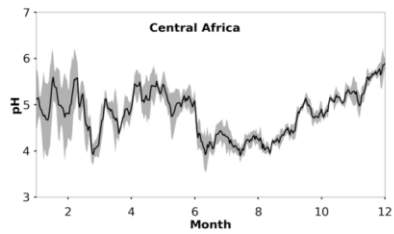
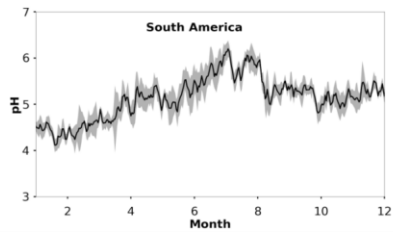
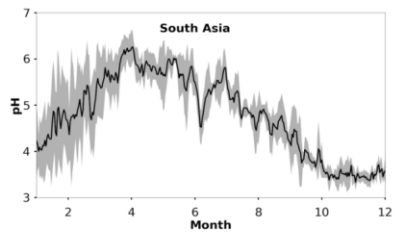
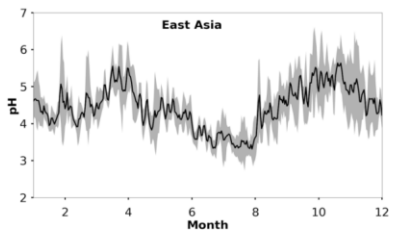
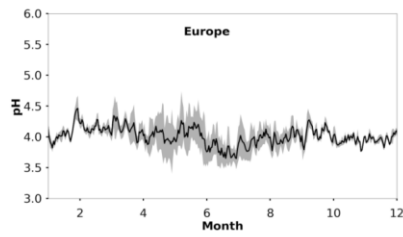
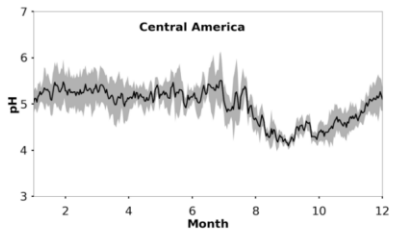
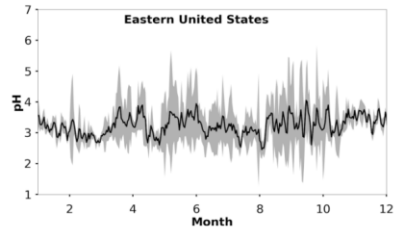
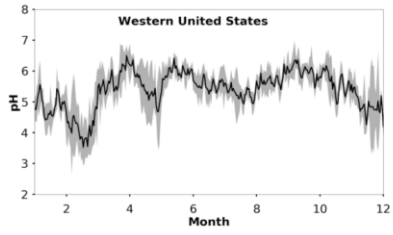


Figure 1: Mean, near-surface fine aerosol pH during the period 2010-2015 (central panel). Surrounding panels show the temporal pH evolution during the period 1970-2020 at locations defined in Table 1. Black lines represent the reference simulation. Red and blue lines show the sensitivity simulations in which crustal particle and NH_3 emissions are removed, respectively. Ranges represent the 1σ standard deviation. The anomaly in 1991/2 is related to the Mt Pinatubo eruption.



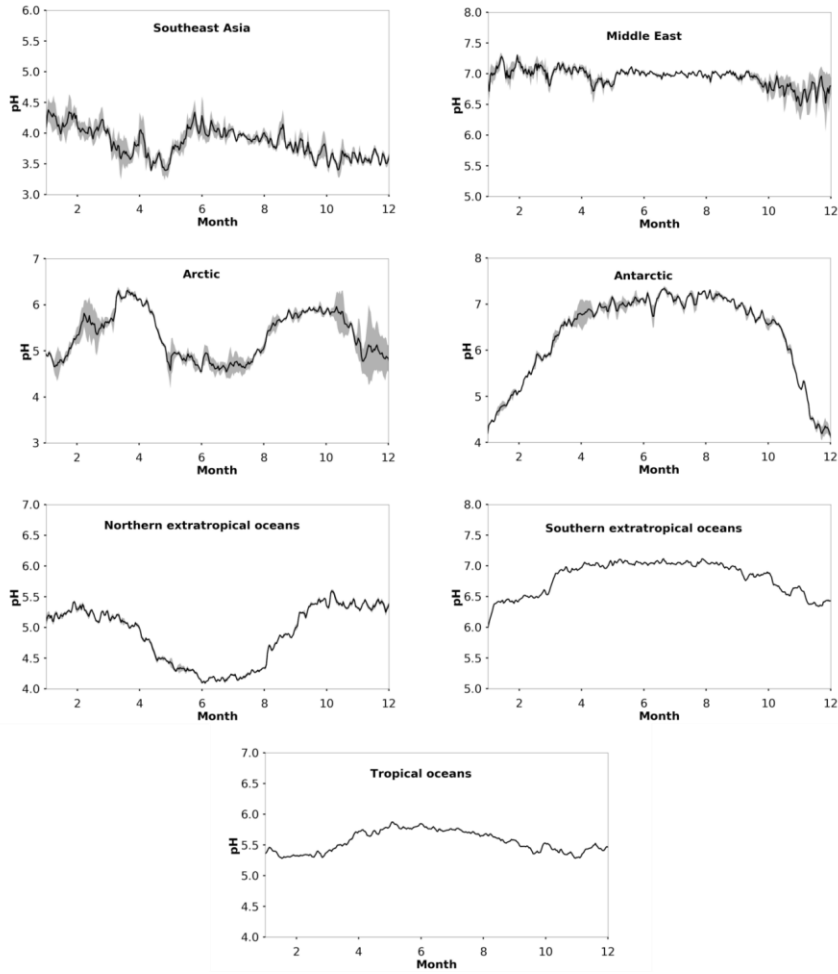


Figure 2: Average seasonal cycle of modelled pH during the period 2010-2015 at locations defined in Table 1. Ranges represent the 1σ standard deviation.

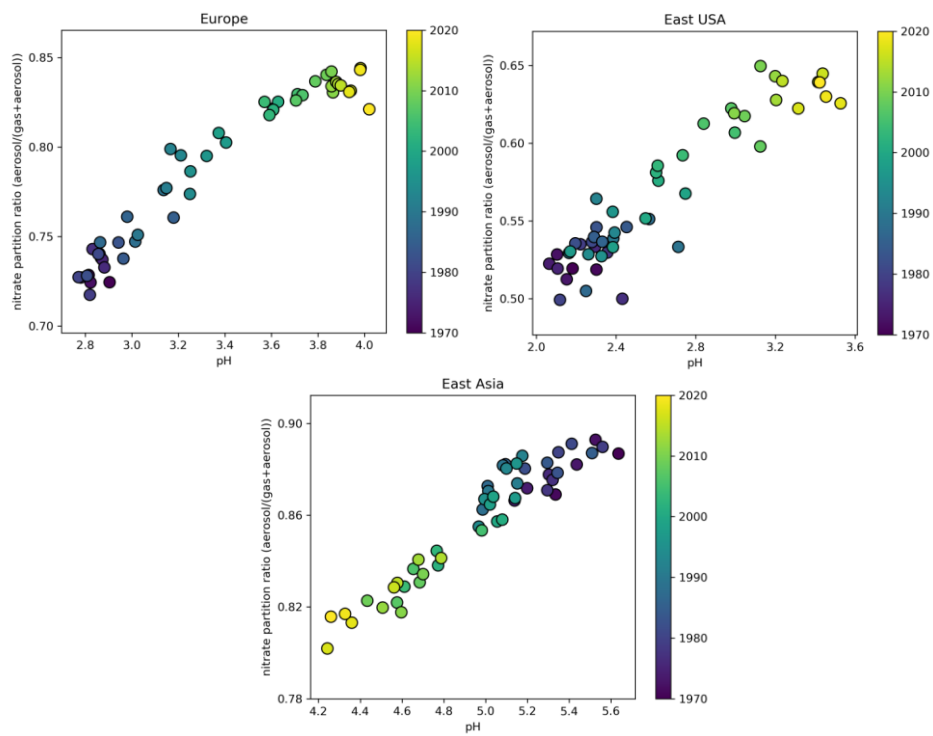


Figure 3: Time evolution of particle phase fraction of total nitrate as a function of pH over Europe (left), the Eastern USA (right) and East Asia (bottom) during the period 1970-2020.

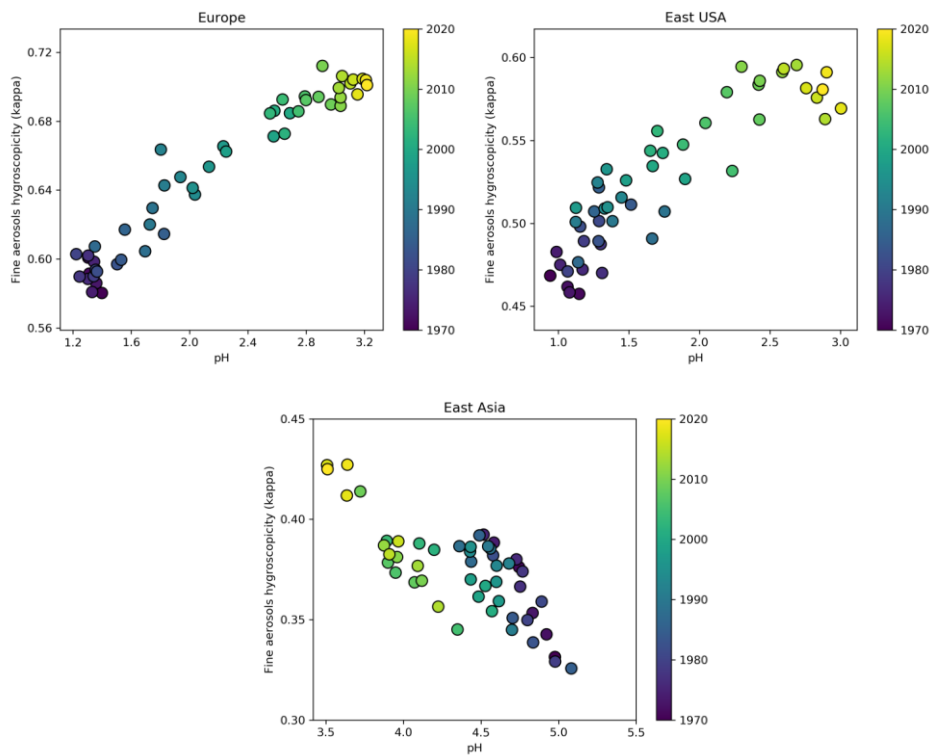


Figure 4: Time evolution of annual average aerosol hygroscopicity (κ) as a function of pH over Europe (left), the Eastern USA (right) and East Asia (bottom) during the period 1970-2020 at the lowest cloud-forming level (940 hPa).

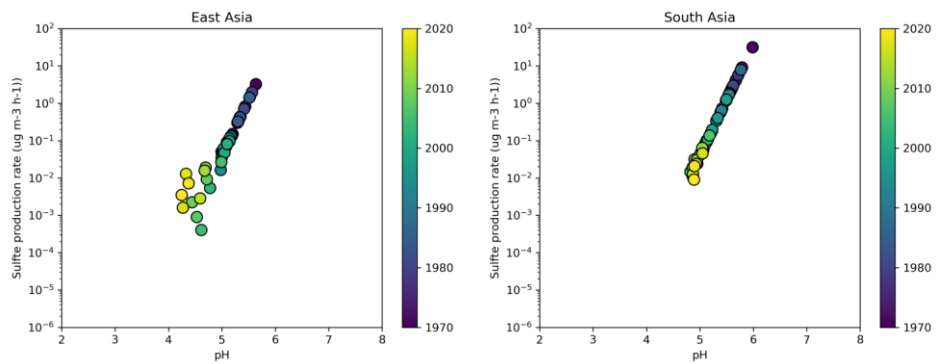


Figure 5: Time evolution of the sulfate production rate on aqueous aerosols from the SO_2+O_3 multiphase chemistry reaction as a function of aerosol pH over East Asia (left) and South Asia (right) during the period 1970-2020.

Table 1: Decadal averages of aerosol pH.

Region	Longitude	Latitude	1971-1980	1981-1990	1991-2000	2001-2010	2011-2020
Western USA ¹	90°-70°W	30°-46°N	4.6	4.8	4.8	5.0	5.1
Eastern USA ¹	124°-114°W	30°-52°N	2.2	2.4	2.4	2.9	3.3
Central America ¹	106°-52°W	4°-28°N	4.6	4.6	4.6	4.7	4.9
Europe ¹	12°W-36°E	34°-62°N	2.8	3.0	3.3	3.7	3.9
East Asia ¹	100°-114°E	20°-44°N	5.3	5.2	5.1	4.7	4.5
South Asia ¹	68°-94°E	8°-32°N	5.6	5.5	5.3	5.0	4.9
South America ¹	75°-35°W	30°-0°S	5.2	5.1	5.1	5.1	5.1
Central Africa ¹	10°-40°E	10°S-10°N	4.9	4.8	4.8	4.7	4.9
Southeast Asia ¹	94°-130°E	12°S-20°N	4.5	4.3	4.1	3.9	3.8
Middle East ¹	36°-60°E	12°-34°N	7.0	7.0	6.9	6.9	6.8
Arctic	0°-360°	60°-90°N	4.2	4.2	4.6	4.8	5.2
North extratropics ²	0°-360°	20°-60°N	4.8	4.8	4.7	4.7	4.9
Tropical oceans ²	0°-360°	20°S-20°N	5.6	5.6	5.5	5.5	5.5
South extratropics ²	0°-360°	60°-20°S	6.8	6.8	6.8	6.8	6.8
Antarctic	0°-360°	90°-60°S	5.9	5.9	5.6	5.8	5.8

¹Only values over land are considered for the calculation of pH

²Only values over oceans are considered for the calculation of pH

Supplementary Materials

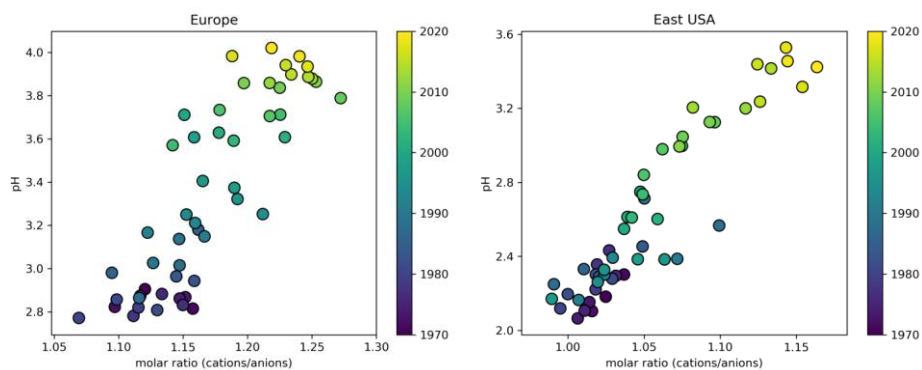


Figure S1: Time evolution of annual average pH as a function of cation/anion molar ratio over Europe (left) and the Eastern USA (right) during the period 1970-2020.

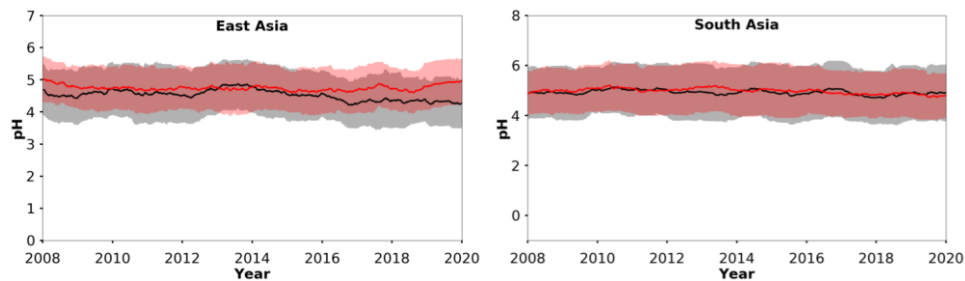


Figure S2: Temporal pH evolution in East and South Asia during the period 2008-2020. Black lines represent the reference simulation. Red lines show the sensitivity simulation in which SO₂ emissions are reduced by 75% in East Asia and increased by 50% in South Asia. Ranges represent the 1σ standard deviation.

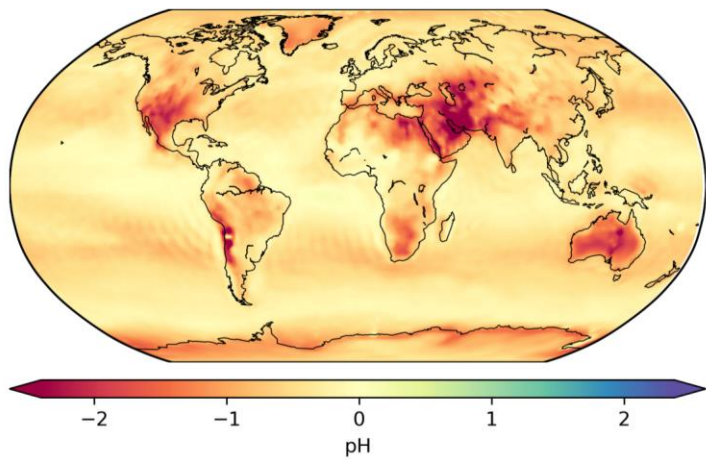


Figure S3: Absolute change in the calculated mean near-surface fine aerosol pH during the period 2010-2015 (cf. central panel in Fig. 1) by assuming that aerosols are always aqueous solution droplets (metastable state). A negative change corresponds to more acidic particles compared to the stable state assumption.

Table S1: Fractional emission factors of aerosol components for biofuel combustion, and savannah and tropical forest biomass burning (Akagi et al., 2011), and for sea salt (Seinfeld and Pandis, 2006).

Location	Latitude	Longitude	Time period	Simulated mean pH	Field-derived mean pH	Method used	Reference
Pellston, MI, USA	45.55°N	84.78°W	Jul 2016	3.8	3.5	pH indicator paper/ colorimetric image	Craig et al., 2018
Ann Arbor, MI, USA	42.28°N	83.74°W	Aug 2016	4.3	3.5	pH indicator paper/ colorimetric image	Craig et al., 2018
Centreville, AL, USA	32.9°N	87.25°W	Jun 1998—Aug 2013	6.4	4.2	ISORROPIA (no-NH ₃)	Weber et al., 2016
Centreville, AL, USA	32.9°N	87.25°W	Jun—Jul 2013	7.0	4.1	ISORROPIA	Pye et al., 2018
Egbert, ON, Canada	44.23°N	79.78°W	Jul—Sep 2012	3.9	2.1	E-AIM-Model II	Murphy et al., 2017
Harrow, ON, Canada	42.03°N	82.89°W	Jun—Jul 2007	4.2	4.6	E-AIM-Model II	Murphy et al., 2017
Pasadena, CA, USA	34.14°N	118.12°W	Jun 2010	5.9	2.7	ISORROPIA (metastable)	Guo et al., 2017
Toronto, Canada	43.66°N	79.40°W	2007-2013	4.0	2.6	E-AIM-I (with gas-NH ₃ , HNO ₃)	Tao and Murphy, 2019
Toronto, Canada	43.66°N	79.40°W	2014-2016	4.1	2.7	E-AIM-I (with gas-NH ₃ , HNO ₃)	Tao and Murphy, 2019
Ottawa, Canada	45.43°N	75.68°W	2007-2016	4.0	2.5	E-AIM-I (with gas-NH ₃ , HNO ₃)	Tao and Murphy, 2019
Simeoe, Canada	42.86°N	80.27°W	2007-2016	4.4	2.41	E-AIM-I (with gas-NH ₃ , HNO ₃)	Tao and Murphy, 2019
Montreal, Canada	45.65°N	73.57°W	2007-2016	4.0	2.4	E-AIM-I (with gas-NH ₃ , HNO ₃)	Tao and Murphy, 2019
Windsor, Canada	42.29°N	83.07°W	2007-2010	4.4	2.1	E-AIM-I (with gas-NH ₃ , HNO ₃)	Tao and Murphy, 2019
Windsor, Canada	42.29°N	83.07°W	2012-2016	4.5	2.4	E-AIM-I (with gas-NH ₃ , HNO ₃)	Tao and Murphy, 2019
St. Anicet, Canada	45.12°N	74.29°W	2007-2016	4.0	2.5	E-AIM-I (with gas-NH ₃ , HNO ₃)	Tao and Murphy, 2019
Sao Paulo, Brazil	23.55°S	46.63°W	Aug—Sep 2012	6.2	4.8	E-AIM	Vieira-Filho et al., 2016

Po-Valley, Italy	45.40°N	12.20°E	Mar-2009—Jan-2010	4.5	3.1	E-AIM-Model-IV	Squizzato et al., 2013
Po-Valley, Italy	45.40°N	12.20°E	Spring-2009	4.3	3.6	E-AIM-Model-IV	Squizzato et al., 2013
Po-Valley, Italy	45.40°N	12.20°E	Summer-2009	4.8	2.3	E-AIM-Model-IV	Squizzato et al., 2013
Po-Valley, Italy	45.40°N	12.20°E	Fall-2009	4.5	3	E-AIM-Model-IV	Squizzato et al., 2013
Po-Valley, Italy	45.40°N	12.20°E	Winter-2009-2010	4.4	3.4	E-AIM-Model-IV	Squizzato et al., 2013
Po-Valley, Italy	45.40°N	12.20°E	Winter-2012-2013	4.2	3.9	ISORROPIA (metastable, no-NH ₃)	Masiol et al., 2020
Po-Valley, Italy	45.40°N	12.20°E	Spring-2012	4.1	2.3	ISORROPIA (metastable, no-NH ₃)	Masiol et al., 2020
Cabauw, Netherlands	51.97°N	4.93°E	Jul-2012—Jun-2013	4.0	3.7	ISORROPIA	Guo et al., 2018
Cabauw, Netherlands	51.97°N	4.93°E	Jun—Aug-2013	3.6	3.3	ISORROPIA	Guo et al., 2018
Cabauw, Netherlands	51.97°N	4.93°E	Dec—Feb-2012	4.1	3.9	ISORROPIA	Guo et al., 2018
Beijing, China	39.99°N	116.30°E	Nov-2015—Dec-2016	4.9	4.2	ISORROPIA	Liu et al., 2017
Guangzhou, China	23.13°N	113.26°E	Jul-2013	2.6	2.5	E-AIM-Model-IV	Jia et al., 2018
Beijing, China	39.97°N	116.37°E	Nov-2014—Dec-2014	4.5	4.6	ISORROPIA	Song et al., 2018
Beijing, China	40.41°N	116.68°E	Oct-2014—Jan-2015	5.6	4.7	ISORROPIA (metastable)	He et al., 2018
Beijing, China	39.99°N	116.31°E	Jan—Dec-2014	4.9	3.0	ISORROPIA (metastable)	Tan et al., 2018
Beijing, China	39.99°N	116.31°E	Winter-2014	5.5	4.1	ISORROPIA (metastable)	Tan et al., 2018
Beijing, China	39.99°N	116.31°E	Fall-2014	6.0	3.1	ISORROPIA (metastable)	Tan et al., 2018
Beijing, China	39.99°N	116.31°E	Spring-2014	5.4	2.1	ISORROPIA (metastable)	Tan et al., 2018

Beijing, China	39.99°N	116.31°E	Summer-2014	3.1	1.8	ISORROPIA (metastable)	Tan et al., 2018
Tianjin, China	39.11°N	117.16°E	Dec-2014—Jun-2015	4.4	4.9	ISORROPIA (metastable)	Shi et al., 2017
Tianjin, China	39.11°N	117.16°E	Aug-2015	1.4	3.4	ISORROPIA (metastable)	Shi et al., 2017
Beijing, China	39.98°N	116.28°E	Feb-2017	4.7	4.5	ISORROPIA	Ding et al., 2019
Beijing, China	39.98°N	116.28°E	Apr—May-2016	5.2	4.4	ISORROPIA	Ding et al., 2019
Beijing, China	39.98°N	116.28°E	Jul—Aug-2017	2.2	3.8	ISORROPIA	Ding et al., 2019
Beijing, China	39.98°N	116.28°E	Sep—Oct-2017	4.5	4.3	ISORROPIA	Ding et al., 2019
Guangzhou, China	23.13°N	113.26°E	Jul—Sep-2013	2.7	2.4	E-AIM-Model-III	Jia et al., 2018
Hohhot, China	40.48°N	111.41°E	Summer-2014	5.5	5	ISORROPIA (metastable, no-NH ₃)	Wang et al., 2019
Hohhot, China	40.48°N	111.41°E	Autumn-2014	6.8	5.3	ISORROPIA (metastable, no-NH ₃)	Wang et al., 2019
Hohhot, China	40.48°N	111.41°E	Winter-2014	5.8	5.7	ISORROPIA (metastable, no-NH ₃)	Wang et al., 2019
Hohhot, China	40.48°N	111.41°E	Spring-2015	6.1	6.1	ISORROPIA (metastable, no-NH ₃)	Wang et al., 2019
Hohhot, China	40.48°N	111.41°E	2014—2015	6.2	5.6	ISORROPIA (metastable, no-NH ₃)	Wang et al., 2019
Beijing, China	40.41°N	116.68°E	Oct-2014—Jan-2015	5.6	7.6	ISORROPIA (stable-state)	He et al., 2018
Xi'an, China	34.23°N	108.89°E	Nov—Dec-2012	5.7	6.7	ISORROPIA	Wang et al., 2016
Beijing, China	39.99°N	116.30°E	Jan—Feb-2015	5.0	7.6	ISORROPIA	Wang et al., 2016
Beijing, China	40.35°N	116.30°E	Jun—Aug-2005	4.2	0.6	E-AIM-Model-II (only-aerosols)	Pathak et al., 2009
Shanghai, China	31.45°N	121.10°E	May—Jun-2005	3.5	0.7	E-AIM-Model-II (only-aerosols)	Pathak et al., 2009

Lanzhou, China	36.13°N	103.68°E	Jun—Jul 2006	6.8	0.6	E-AIM-Model II (only aerosols)	Pathak et al., 2009
Beijing, China	40.32°N	116.32°E	Jan 2005—Apr 2006	5.1	0.7	E-AIM-Model II (only aerosols)	He et al., 2012
Chongqing, China	29.57°N	106.53°E	Jan 2005—Apr 2006	3.6	1.5	E-AIM-Model II (only aerosols)	He et al., 2012
Beijing, China	40°N	116.33°E	Jan 2013	4.6	5.8	ISORROPIA (forward & reverse, estimated NH ₃)	Wang et al., 2016
Singapore	1.3°N	103.78°E	Sep—Nov 2011	3.2	0.6	E-AIM-Model IV	Behera et al., 2013
Hong-Kong	22.34°N	114.26°E	Jul 1997—May 1998	3.3	0.3	E-AIM-Model II (for RH >= 70%)	Yao et al., 2007
Hong-Kong	22.34°N	114.26°E	Nov 1996—Nov 1997	3.4	-1	E-AIM-Model II (for RH < 70%)	Yao et al., 2007
Hong-Kong	22.34°N	114.26°E	Oct 2008	5.0	0.6	E-AIM-Model III (only aerosols)	Xue et al., 2011
Hong-Kong	22.34°N	114.26°E	Nov 2008	3.7	-0.5	E-AIM-Model III (only aerosols)	Xue et al., 2011
Hong-Kong	22.34°N	114.26°E	Jun—Jul 2009	1.6	-0.1	E-AIM-Model III (only aerosols)	Xue et al., 2011
Pacific Ocean	47.5°S	147.5°E	Nov—Dec 1995	7.0	1.0	EQUISOLV	Fridlind and Jacobson, 2000
South Ocean	61°S	45°W	Jan 2015	6.9	1.4	ISORROPIA (no-NH ₃)	Dall'Osto et al., 2019
South Ocean	64°S	65°W	Jan—Feb 2015	6.9	3.8	ISORROPIA (no-NH ₃)	Dall'Osto et al., 2019

Table S2: Fractional emission factors of aerosol components for biofuel combustion, and savannah and tropical forest biomass burning (Akagi et al., 2011), and for sea salt (Seinfeld and Pandis, 2006).

Source	SO ₄ ²⁻	NO ₃ ⁻	Cl ⁻	Na ⁺	K ⁺	Mg ²⁺	Ca ²⁺	NH ₄ ⁺
Biofuel combustion	-	0.014	-	-	0.093	0.022	0.073	-
Grassfire burning	0.05	0.04	0.62	0.01	0.62	0.04	0.06	0.01
Forest fire burning	0.25	0.21	0.29	0.01	0.56	0.08	0.16	0.01
Sea salt	0.077	-	0.55	0.306	0.011	0.037	0.012	-

Table S3: Fractional chemical composition of mineral dust emissions (Karydis et al., 2016).

Desert	Na ⁺	K ⁺	Ca ²⁺	Mg ²⁺	Other
Great Basin	0.064	0.023	0.053	0.018	0.842
Mojave	0.015	0.027	0.059	0.019	0.880
Sonoran	0.025	0.012	0.037	0.006	0.920
Patagonia	0.012	0.015	0.021	0.013	0.939
Monte	0.023	0.018	0.025	0.009	0.925
Atacama	0.069	0.007	0.018	0.005	0.901
Kalahari/ Namibia	0.030	0.050	0.120	0.090	0.710
Sahara	0.011	0.035	0.075	0.030	0.849
Saudi Arabia	0.010	0.004	0.034	0.006	0.946
Thar/Lut	0.022	0.033	0.082	0.022	0.841
Taklimakan	0.012	0.030	0.120	0.028	0.810
Gobi	0.012	0.021	0.077	0.017	0.873
Great Sandy/ Simpson	0.028	0.001	0.005	0.003	0.963
Other	0.012	0.015	0.024	0.009	0.940

Formatted: Font: 9 pt, English (United States)

Formatted: Indent: Left: 0 cm, Hanging: 0.63 cm, Tab stops: Not at 3.23 cm